Computers and Chemical Engineering 204 (2026) 109388

Contents lists available at ScienceDirect

Computers and Chemical Engineering

journal homepage: www.elsevier.com/locate/cace

Simultaneous design of microbe and bioreactor

Anita L. Ziegler [a], Marc-Daniel Stumm [a], Tim Prömper [a], Thomas Steimann [b], Jørgen Magnus [b], Alexander Mitsos [c,a,d,*]

[a] Process Systems Engineering (AVT.SVT), RWTH Aachen University, Aachen, 52074, Germany
[b] Biochemical Engineering (AVT.BioVT), RWTH Aachen University, Aachen, 52074, Germany
[c] JARA-ENERGY, Aachen, 52056, Germany
[d] Institute of Climate and Energy Systems, Energy Systems Engineering (ICE-1), Forschungszentrum Jülich GmbH, Jülich, 52425, Germany

ARTICLE INFO

Dataset link: https://git.rwth-aachen.de/avt-svt/public/simulknock

Keywords:
Bioreactor design
Computational strain design
Metabolic modeling
Continuous fermentation
Techno-economic analysis

ABSTRACT

When developing a biotechnological process, the microorganism is first designed, e.g., using metabolic engineering. Then, the optimum fermentation parameters are determined on a laboratory scale, and lastly, they are transferred to the bioreactor scale. However, this step-by-step approach is costly and time-consuming and may result in suboptimal configurations. Herein, we present the bilevel optimization formulation *SimulKnockReactor*, which connects bioreactor design with microbial strain design, an extension of our previous formulation, SimulKnock (Ziegler et al., 2024). At the upper (bioreactor) level, we minimize investment and operation costs for agitation, aeration, and pH control by determining the size and operating conditions of a continuous stirred-tank reactor—without selecting specific devices like the stirrer type. The lower (cellular) level is based on flux balance analysis and implements optimal reaction knockouts predicted by the upper level. Our results with a core and a genome-scale metabolic model of *Escherichia coli* show that the substrate is the largest cost factor. Our simultaneous approach outperforms a sequential approach using OptKnock. Namely, the knockouts proposed by OptKnock cannot guarantee the required production capacity in all cases considered. SimulKnockReactor, on the other hand, provides solutions in all cases considered, highlighting the advantage of combining cellular and bioreactor levels. This work is a further step towards a fully integrated bioprocess design.

1. Introduction

Model-based simulation and optimization are established methods for the design and scale-up of fermentation processes. When modeling a fermentation process, different scales and their respective variables and parameters come into play, e.g., the cellular level, the fermentation reaction level, and the bioreactor level (Pinto et al., 2016; Villadsen et al., 2011).

At the cellular level, the intracellular fluxes can be determined via metabolic modeling, typically via flux balance analysis (FBA) (Orth et al., 2010b; Watson, 1986; Savinell and Palsson, 1992), which is based on steady-state mass balances of the intracellular metabolites. The metabolites and their corresponding reaction stoichiometry are contained in the genome-scale metabolic model (GEM) of the microorganism. With evolving available information in the GEM, different aspects have been included in metabolic modeling formulations, e.g., the intracellular pH (Du et al., 2019), thermodynamics (Niebel et al., 2019), and regulatory aspects, reviewed by Gombert and Nielsen (2000). First introduced by Burgard et al. (2003), numerous strain optimization formulations have been developed, that allow for predicting optimal genetic modifications for improved product yield.

At the fermentation reaction level, the concentrations of the representative extracellular compounds are described by mass balances together with whole-cell growth or enzyme kinetics. Often energy balances are also required. Momentum balances can be set up (Liu, 2020) but typically lumped models are used. In the most basic case, the representative compounds are biomass, substrate, and product. Depending on the fermentation mode, e.g., batch, fed-batch, or continuous, the mass balances are differential, algebraic, or differential–algebraic equations (Chmiel et al., 2018; Bailey and Ollis, 1986). Exemplary fermentation parameters are temperature, pH, and nutrient composition (Rao et al., 2006; Porto de Souza Vandenberghe et al., 2022). Gordeeva et al. (2013) presented one of the few examples of optimal fermentation design, namely for continuous fermentation including a recycling stream. Another example was presented by Sinner et al. (2019), who proposed a bi-objective optimization formulation for maximal space–time yield

* Corresponding author at: Process Systems Engineering (AVT.SVT), RWTH Aachen University, Aachen, 52074, Germany.
E-mail address: amitsos@alum.mit.edu (A. Mitsos).

https://doi.org/10.1016/j.compchemeng.2025.109388
Received 10 July 2025; Received in revised form 27 August 2025; Accepted 31 August 2025
Available online 22 September 2025

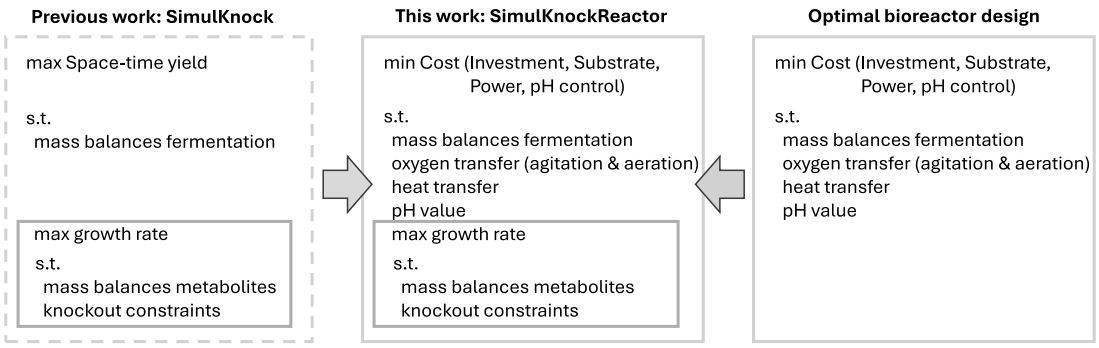

Fig. 1. Overview of the elements of SimulKnock (Ziegler et al., 2024) and optimal bioreactor design that were combined to create the proposed formulation SimulKnockReactor in this work. The bilevel structure is adopted from SimulKnock: the lower level remains unchanged; the upper level is extended to include optimal bioreactor design. Note that optimal bioreactor design is not standard in the literature, however, the incorporated equations can largely be found in standard bioreactor and bioreaction literature (Doran, 1995; Villadsen et al., 2011; Chmiel et al., 2018; Liu, 2020).

and minimal sugar concentration in the effluent of continuous fermentation. To ensure and boost the performance of the fermentation, however, it is fruitful to connect the cellular level with the process levels (Richelle et al., 2020; Olsson et al., 2022). Mahadevan et al. (2002) were the first to connect the fermentation reaction level with the cellular level in their dynamic flux balance analysis. Chang et al. (2016), Jabarivelisdeh et al. (2020), and Bhonsale et al. (2022) extended this connection to model-predictive control of the fermentation, similar to de Oliveira et al. (2021) and Espinel-Ríos and Avalos (2024), who used machine learning techniques for substituting the cellular level. Zhuang et al. (2013) considered yield, titer, and space–time yield for batch and fed-batch fermentation with product inhibition in their iterative strain design approach. Jabarivelisdeh and Waldherr (2018) also maximized the space–time yield, namely in a dynamic bilevel optimization program, switching on genetic modifications that were found in the preceding step. In our previous work (Ziegler et al., 2024), we combined strain optimization with optimal fermentation design. In our bilevel optimization formulation *SimulKnock*, the upper (fermentation) level includes the mass balances of continuous fermentation, while the lower (cellular) level is derived from FBA. SimulKnock was solved for two case studies with the GEM *i*ML1515 (Monk et al., 2017) of *E. coli* embedded. The results indicated that different knockouts were found and that the space–time yield could be significantly elevated compared to sequential optimization. This sequential optimization represents the common practice of first optimizing the microbial strain and then, subsequently, optimizing the fermentation. The optimization formulation SimulKnock, however, focuses on the cellular and the fermentation reaction level and does not give any information about the bioreactor level, including sizing of the bioreactor and cost.

At the bioreactor level, in principle, the selection of reactor types, economic evaluation, and scale-up aspects become important (Posten, 2018; Clarke, 2013), to give a comprehensive list. The selection of reactor type includes stirred tank reactors, pneumatically driven reactors, and other types (Posten, 2018). Economic evaluation includes operating costs, material costs, separation costs, and product value, among others (Liu, 2020; Doran, 1995). So far, the idea behind scale-up is to find suitable fermentation conditions at the laboratory scale and transfer these to the industrial bioreactor scale (Porto de Souza Vandenberghe et al., 2022; Clarke, 2013). Based on the parameters of the fermentation reaction, e.g., temperature and pH, the scale-up aspects are mechanical agitation, aeration, heat transfer, power consumption, rheology, and biotransformation (Rao et al., 2006; Villadsen et al., 2011; Mandenius, 2016). Computational fluid dynamics have been used to model the spatial distribution of compounds in the bioreactor (Kelly, 2008; Rathore et al., 2016). Cardoso et al. (2020) and Knoll et al. (2005) estimated bioreactor costs for different cultivation conditions. In optimal control, Hebing et al. (2020) considered the oxygen transfer rate, and von Stosch et al. (2016) also included data on temperature, pH, and agitation rate measurement in their hybrid modeling approach. With fixed reactor volume, Powell and Hill (2008) chose a bioreactor setup and reduced cost in an iterative process. Nath and Das (2011) reviewed factorial design methods for improved hydrogen production. Interestingly, we did not find studies that used numerical optimization for optimal bioreactor design.

In summary, the field of model-based optimal bioreactor design and cost estimation of bioreactors is underrepresented in biochemical engineering and, more specifically, the bioreactor level and the cellular level are yet to be connected. In industrial applications, strain design and bioreactor design are even performed by separate groups. This connection of the two fields, however, is crucial in our eyes in order to design economically viable processes. An organism that reaches a high product yield and even a high space–time yield might not prove economically reasonable in an industrial bioreactor because other aspects like substrate cost and operation cost become decisive at the bioreactor level. In another case, the optimal fermentation conditions of the laboratory scale prove to not be realizable in the bioreactor. With the usual approach of optimizing the microbe, the fermentation conditions, and the bioreactor one after the other, it is necessary in these cases to go back and redevelop the microbial strain and the fermentation conditions, which is costly and time-consuming. By connecting strain design with fermentation and bioreactor design, we can circumvent this loop and simultaneously optimize the strain for the reactor and vice versa.

Herein, we present *SimulKnockReactor*, a methodology for bioreactor cost optimization considering gene deletion strategies. It combines bioreactor design with strain design in a bilevel optimization formulation and is an extension of our recent contribution SimulKnock (Ziegler et al., 2024). Within SimulKnockReactor, the lower level calculates the intracellular fluxes based on FBA, analogous to SimulKnock. The genetic modification, which we focus on, is gene deletion. The upper level of SimulKnockReactor minimizes the cost of a bioreactor based on capital expenditures (CAPEX) and operational expenses (OPEX)—in contrast to SimulKnock, where the space–time yield was maximized. The bioreactor is modeled as a set of mass and energy balances, combined with cost correlations. We estimate the cost for a stirred-tank reactor, for substrates, oxygen supply, heat transfer, and pH regulation. We do not select specific devices of the bioreactor and the surrounding equipment; for example, we do not distinguish between a cooling jacket and a cooling coil or different stirrer types. Despite this fact, we still use the term bioreactor design throughout this work, since we do calculate the mass and energy flow rates of the fermentation, and the required mass flow rates of pH control agents, air, and cooling agent. Moreover, based on these flows, the required power for pumping, stirring, and compression, as well as the sizing of the reactor are determined. Information about oxygen and substrate consumption, biomass and product generation are retrieved from the lower (cellular) level. This approach

is expected to improve the accuracy compared to common correlations and allows to examine a specific organism without experimental setup. As exemplary case studies, we apply SimulKnockReactor to a core network and a GEM of *E. coli* for aerobic production of formate, acetate, and succinate and compare the reaction deletions with SimulKnock results. As discussed in the outlook, the reactor design could be extended to account for other aspects.

The contribution of this work is to provide a methodology for the initial assessment of bioreactor costs, reactor sizing, and operation, and simultaneously, the prediction of optimal gene deletions. The outstanding feature of the methodology is to connect the micro- and the macro-level of a bioprocess, or, in other words, the field of microbial strain design with bioreactor design. Our methodology is applicable to diverse microorganisms and target chemicals. Thus, this work is the next step towards a fully integrated bioprocess design, considering all levels of bioprocess engineering.

2. Method: Simultaneous bioreactor design and microbial strain design

Our aim was to minimize the cost of a bioreactor based on process variables and reaction knockouts concerning the microbial fluxes. The cost of the bioreactor consists of CAPEX and OPEX, of which we considered the aspects of aeration, agitation, pH control, and cooling. To calculate these costs, a model of the bioreactor and the surrounding equipment is needed which includes the compounds of the fermentation. The fermentation, in turn, is coupled with the microbial metabolism by the uptake and secretion reactions of the organism. Our previous formulation SimulKnock (Ziegler et al., 2024) already represents a framework where the fermentation equations are coupled with the metabolic fluxes. In bilevel optimization, one optimization program which is called a lower-level program is embedded in another optimization program, which is called an upper-level program (Dempe, 2002). In this work, we build upon SimulKnock by extending the model to allow for optimal bioreactor design. Fig. 1 depicts the elements of SimulKnock and optimal bioreactor design and how we combined them to form SimulKnockReactor.

We retained the bilevel structure and the lower level of SimulKnock (see Fig. 1, left side) and extended the upper level of SimulKnock with a formulation of optimal bioreactor design. As a result, the objective of optimization changes from maximizing the space–time yield to minimizing costs. Moreover, we included more fermentation compounds, namely oxygen, hydrogen, and strong ions.

In contrast to a formulation of optimal bioreactor design (see Fig. 1, right side), which is single-level, we used the lower-level variables instead of applying commonly used correlations. This replacement is possible because the metabolic network includes exchange reactions that connect the metabolism to the environment, i.e., the fermentation culture. These uptake and excretion reactions are also part of the bioreactor equations. By using lower-level variables in the upper level, we connected the bioreactor level with the cellular level.

In the following, the previous formulation of SimulKnock is described. Then, the objective and constraints for bioreactor design are introduced and merged with SimulKnock in the next step. The implementation and solution of the resulting bilevel formulation with global and local optimization techniques are shown in the last section of this chapter.

2.1. Previous work: Simultaneous design of fermentation and microbe

The bilevel optimization formulation SimulKnock (Ziegler et al., 2024) simultaneously optimizes a continuous fermentation process and a microbial strain for growth-coupled production. The upper level of SimulKnock represents the fermentation level, while the lower level represents the cellular level. The connection between the upper and the lower levels is achieved via the implementation of kinetics and via the replacement of common correlations with cellular variables. We provide an overview of the SimulKnock formulation in the following and refer the interested reader to our previous publication (Ziegler et al., 2024) for details and assumptions. The mathematical formulation of SimulKnock with the embedded Monod kinetics reads

$$\max_{\substack{y,c_{S,Feed},c_P,\\ c_{bio},v'_S,v'_{bio},v'_P}} \quad c_P \cdot v'_{bio} \quad \rightarrow \text{maximize space–time yield} \tag{1}$$

$$\text{s.t. } \kappa \geq \sum_{i=1}^{r}(1-y_i) \rightarrow \text{maximum number of knockouts} \tag{2}$$

$$0 = -v'_S \cdot M_S \cdot c_{bio} + v'_{bio} \cdot \left(c_{S,Feed} - K_S \frac{v'_{bio}}{v^{max}_{bio} - v'_{bio}}\right) \quad \rightarrow \text{mass balance substr. conc.} \tag{3}$$

$$0 = v'_P \cdot M_P \cdot c_{bio} - c_P \cdot v'_{bio} \quad \rightarrow \text{mass balance product conc.} \tag{4}$$

$$\boldsymbol{v'} \in \arg\max_{\boldsymbol{v}} \quad v_{bio} \quad \rightarrow \text{maximize growth} \tag{5}$$

$$\begin{aligned} \text{s.t.} \quad \boldsymbol{S}\boldsymbol{v} &= \boldsymbol{0} && \rightarrow \text{mass balances metabolites} \\ v_{bio} &\geq f \cdot v_{bio,WT} && \rightarrow \text{biomass threshold} \\ \boldsymbol{v} &\geq \boldsymbol{v^{lower}} \circ (\boldsymbol{B}\boldsymbol{y}) && \rightarrow \text{knockout constraints} \\ \boldsymbol{v} &\leq \boldsymbol{v^{upper}} \circ (\boldsymbol{B}\boldsymbol{y}), && \rightarrow \text{knockout constraints} \end{aligned} \tag{6}$$

with c standing for concentration, v being microbial fluxes, and $\boldsymbol{y} \in \{0,1\}^r$ denoting the binary knockout vector. The units of the variables and parameters can be found in the Nomenclature. The size r of the vector $\boldsymbol{y}$ corresponds to the number of reactions in the metabolic network. In SimulKnock and also throughout this work, we refer to "knockout" as "reaction elimination". The subscripts S, P, bio, and WT denote the substrate, the product, the biomass, and the wild-type, respectively. The biomass flux of the strain before genetic modification $v_{bio,WT}$ is a reference flux and can be either determined experimentally or via FBA. The superscript apostrophe $'$ formally designates the lower-level variables in the upper level; i denotes the summation index. The parameters κ, M, K_S, and f stand for the fixed maximum allowable number of knockouts, the molar mass, the Monod constant, and a fixed number between zero and one ensuring a minimal biomass production, respectively. The tabulated parameter values can be found in Table A.1. The stoichiometric matrix $\boldsymbol{S}$ includes the stoichiometric coefficients of each intracellular reaction, where reversible reactions are split into an irreversible forward and an irreversible backward reaction. Accordingly, the mapping matrix $\boldsymbol{B}$ maps reversible reactions with their irreversible counterparts.

In the upper-level program (Eqs. (1)–(4)), the space–time yield of the fermentation is maximized. From continuous fermentation and the mass balance of biomass, it follows that the dilution rate equals the growth rate v_{bio}, which explains why the growth rate v'_{bio} is part of the space–time yield formula. The maximization is subject to two equality constraints, which originate from the mass balances of the substrate (Eq. (3)) and product concentration (Eq. (4)). Further, the upper level contains one inequality constraint (Eq. (2)) to ensure that a maximum allowable number of knockouts κ (with κ as an input parameter) is not exceeded, which is a standard equation from optimal strain design. The degrees of freedom are the reaction knockouts $\boldsymbol{y}$ and the substrate feed concentration $c_{S,Feed}$.

The upper-level program is also subject to the optimality of the lower-level program (Eqs. (5)–(6)), which is based on FBA and aligns with the lower-level program of OptKnock (Burgard et al., 2003). The lower-level objective is to maximize growth subject to the mass balances of the metabolites, a biomass threshold, and the knockout constraints. The fluxes $\boldsymbol{v}$ are the degrees of freedom to the lower level.

The main assumptions of SimulKnock are that the fermentation culture is ideally mixed, that the metabolism adapts infinitesimally quickly to changed fermentation conditions (Stephanopoulos et al., 1998), and that the kinetic parameters are not affected by the genetic modifications.

2.2. Bioreactor design for minimized cost

We modeled a continuous stirred-tank reactor (CSTR) for aerobic fermentation, including pH control, aeration, and cooling. We kept the assumptions of SimulKnock, in specific also the assumption of an ideally mixed fermentation culture. Therefore, the bioreactor model is a set of integral mass and energy balances, which was combined with cost correlations. Due to the envisaged connection with the cellular level, cellular variables were introduced into the bioreactor design equations. The instances where we performed these replacements will be highlighted in the text. Fig. 2 depicts the aspects that were considered for bioreactor design.

We focused on the bioreactor, i.e., neither considered upstream nor downstream operations. Upstream operations would include sterilization of the substrate, media preparation, or filtration of the air. Downstream operations would include the purification of the product. Considering the bioreactor represents a first step, as adding upstream and downstream units would further increase the complexity. Furthermore, the fermentation may represent the biggest OPEX cost factor in large-scale operation (Nieto et al., 2020). Moreover, we did not consider operating labor costs. In Fig. 2(b), the considered control volumes within the bioreactor are depicted. We ignored the volume of the baffles, the mixer, the sparger, and other internal tubing because they are small compared to the presented control volumes in the production scale.

The economic viability of a bioprocess depends on its production cost. We minimize the hourly production cost, which is composed of CAPEX and OPEX. We assumed CAPEX to be represented by the investment cost of the bioreactor and the compressor; while we assumed the capital cost of the pump to be negligible. For calculating OPEX, we considered raw material costs of the cooling agent, the substrate, and the pH control; as well as power. We assumed the costs of mineral salts to be low compared to substrate costs. We considered air for aeration and assumed that air is free of charge. Further, we assumed that due to the continuous operation, no sterilization and maintenance of the reactor is needed.

$$\begin{aligned}\text{Cost} = &\underbrace{\frac{C_R + C_{compress}}{t_{annual} \cdot t_{amortization}}}_{\text{Investment}} + \underbrace{\frac{\dot{m}_{cooling}}{\rho_{cooling}} C_{cooling}}_{\text{Cooling agent}} \\ &+ \dot{V}(\underbrace{C_S\, c_{S,Feed}}_{\text{Substrate}} + \underbrace{C_{acid}\, M_{acid}\, c_{acid} + C_{base}\, M_{base}\, c_{base}}_{\text{pH control}}) \\ &+ \underbrace{C_{Power}\,\left(P_{compress} + P_{agitation} + P_{cooling}\right)}_{\text{Power}}, \end{aligned} \tag{7}$$

where t denotes the time, C denotes the specific costs; $\dot{m}$ stands for mass flow; ρ stands for density, and $\dot{V}$ stands for the volumetric hourly reactor outflow. The power input is denoted with P. The subscript R stands for the reactor, and *compress* stands for compression, whereas *acid* and *base* in the subscript denote the acid and base of the pH control, respectively. Sulfuric acid was chosen as the acidic pH control component, and sodium hydroxide as the basic pH control component. The specific costs C_S, C_{acid}, C_{base}, and C_{Power} as well as $t_{amortization}$ and t_{annual} are parameters; the values that were used for this work are tabulated in Table A.2.

The reactor investment cost was calculated based on the principle of economy of scale (Powell and Hill, 2008; Perry and Green, 2008) in Eq. (8). Therein, we ignored the inflation factor since we assumed that inflation is balanced out by cheaper production. Further, we ignored CAPEX for media tanks, filters, or seed tanks, which can be associated with the reactor (Negulescu et al., 2023). The investment cost for the compressor was calculated using the equation from Luyben (2018) in Eq. (9), based on Guthrie's correlations (Douglas, 1988).

$$C_R = C_{R,ref} \left(\frac{V_R}{V_{R,ref}}\right)^{0.6} \tag{8}$$

$$C_{compress} = 5840\, P_{compress}^{0.82}, \tag{9}$$

where the subscript ref denotes a reference state. Below the reference volume $V_{R,ref}$, the hourly cost was set equal to $C_{R,ref}$. Again, the chosen values for the parameters, that is, $C_{R,ref}$ and $V_{R,ref}$, can be found in Table A.2.

In Eq. (10), the reactor volume was related to the fermentation culture volume. The hourly reactor outflow $\dot{V}$ was related to the culture volume and was calculated from the annual production capacity (Garcia-Ochoa et al., 2011) by:

$$V_R = \beta \cdot (V_{culture} + V_{gas}) \tag{10}$$

$$V_{culture} = \frac{\dot{V}}{\upsilon_{bio}} \tag{11}$$

$$\dot{V} = \frac{m_{P,annual}}{t_{annual} \cdot c_P} \tag{12}$$

$$V_{culture} = \frac{\pi}{4} D^2 H_{culture} \tag{13}$$

$$H_{culture} = q \cdot D, \tag{14}$$

where V denotes volume and the produced mass is denoted with m; D for diameter, and H for the height of the fermentation culture. The multiplier β accounts for the reactor volume V_R being larger than the culture volume $V_{culture}$ due to a headspace volume (Van't Riet and Tramper, 1991) and the multiplier q relates the height to the diameter of the culture (see Table A.2 for chosen values). In Eq. (11), the dilution rate was replaced by the growth rate υ_{bio}, due to continuous fermentation conditions. With the growth rate being a variable of the cellular level, a bioreactor parameter was replaced with a cellular variable.

As comes clear from Eqs. (13)–(14), we assumed the fermentation culture to be of cylindrical shape, just like the reactor. Together with Eq. (10), the size of the reactor is determined during optimization, which is referred to as optimal bioreactor design.

Numbering-up of reactors

To take into account large production capacities with a maximum standard tank size (Powell and Hill, 2008) and to avoid large spatial distributions (dead zones), we implemented an optional parallel setup of reactors, called numbering-up. For numbering-up, Eq. (15) instead of Eq. (11) is chosen.

$$V_{culture} \cdot n_R = \frac{\dot{V}}{\upsilon_{bio}}, \tag{15}$$

where n_R is the number of reactors set up in parallel. An upper bound on the number of reactors was set to $n_R^{upper} = 10$; an upper bound on the reactor size was set to $V_R^{upper} = 10\,\mathrm{m}^3$. Only at a production capacity of $10^6\,\mathrm{kg\,a^{-1}}$, the maximum number of reactors was set to 100 and the maximum reactor volume to $100\,\mathrm{m}^3$, respectively. Whether the numbering-up option becomes active depends on the production rate chosen.

In the following, the terms for pH control, aeration, and cooling are described in detail.

pH control

The pH level is a decisive factor for the growth and productivity of a microbial strain Parhad and Rao (1974) and, hence, pH control is an integral part of a bioprocess. The pH in fermentation cultures can be distinguished into extracellular and intracellular pH (Straathof, 2023). In this work, we focused on the extracellular pH. The extracellular pH impacts different aspects of a bioprocess, e.g., growth, product formation, and maintenance requirements in the cell (Straathof, 2023). Of these impacts, we chose to model the impact of pH on growth for three reasons. First, even if exemplary publications exist, e.g., for modeling maintenance requirements (Du et al., 2019), strain-wide data are not available yet. Finding a general model for the influence of pH which applies to several strains and several products proved to be difficult.

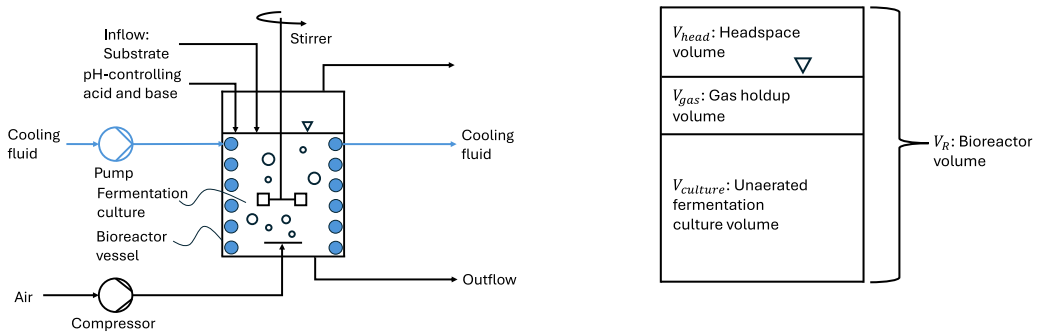

(a) Modeled aspects of a bioreactor (b) Considered control volumes

Fig. 2. Cross section of a continuous stirred-tank bioreactor with the aspects considered in this work in Subfigure (a). The cooling system is depicted in blue color. Subfigure (b) depicts the different control volumes considered in this work. The unaerated fermentation culture volume and the gas holdup volume were artificially separated in this depiction.

Second, the optimization would be further restricted, for example, by implementing a Luedeking-Piret equation or similar for inhibited product formation. Third, like SimulKnock, this work is also based on growth-coupled production, which already links growth with product formation via the GEM. By varying the pH and modeling the impact on growth, we assumed that the predicted genetic modifications would not affect the organism's behavior towards changing pH conditions.

In the absence of experimental data, the extracellular pH was modeled based on the simplified definition of pH (Eq. (16)) and on the idea of a charge balance by Campos and Flotats (2003). We conducted preliminary studies, which were in alignment with Silverstein (2000), who argued that the impact of weak ions is usually smaller than the impact of strong ions. Hence, we only considered the strong ion balance for pH calculation as follows

$$pH = -\log_{10} c_{H^+} \tag{16}$$

$$c_{H^+} = \underbrace{\frac{c_{bio}}{v_{bio}}\left(\sum_i^{n_{acid,strong}} v_i - \sum_i^{n_{base,strong}} v_i\right)}_{\text{strong ion balance}} + \underbrace{c_{acid} - c_{base}}_{\text{pH control}}, \tag{17}$$

where c_{H^+} denotes the equilibrium concentration of hydrogen ions.

Eq. (17) shows that we replaced the concentrations of the acid and base in the fermentation culture with their respective fluxes from the cellular level such that $c_i = \frac{c_{bio}}{v_{bio}} \cdot v_i$. As the extracellular pH was modeled, only fluxes of so-called exchange reactions were taken into account. Exchange reactions denote reactions in the GEM that connect the extracellular with the intracellular space.

The impact of pH on growth can be modeled by adapting kinetic models (Nath and Das, 2011; Straathof, 2023; Wang and Wan, 2009); however, they mostly require experimental data. We introduced an inhibition factor (Zwietering et al., 1993), depicted in Eq. (18) using the cardinal pH model (CPM) (Rosso et al., 1995) in Eq. (19).

$$v_{bio}^{max} = \gamma\, v_{bio}^{opt} \qquad \text{for all } pH^{min} < pH < pH^{max} \tag{18}$$

$$\gamma = \frac{(pH - pH^{min})(pH - pH^{max})}{(pH - pH^{min})(pH - pH^{max}) - (pH - pH^{opt})^2}, \tag{19}$$

where γ is the growth inhibition factor, and pH^{min}, pH^{max}, and pH^{opt} indicate strain-specific parameters for the minimum, the maximum, and the optimum pH, respectively. The growth rate v_{bio}^{opt} denotes the maximum growth rate at optimal pH, which corresponds to the parametric value of v_{bio}^{max} in SimulKnock (Eq. (3)). Below pH^{min} and above pH^{max}, the growth rate v_{bio} is zero. Since growth rates equal to or close to zero are techno-economically not sensible, we set upper and lower bounds on the pH variable, namely pH^{lower} and pH^{upper}. These bounds are tighter than the parameters pH^{min} and pH^{max}, respectively, and represent the vital zone of the organism. As a side-effect, by using these bounds, we could avoid implementing a logical constraint resulting from Eq. (18). We chose the CPM model due to its wide applicability to many microbial strains and due to its small number of additional parameters, i.e., pH^{min}, pH^{max}, and pH^{opt}, which can be found in the literature.

To sum up, we modeled the pH based on the exchange fluxes of the cellular level, with a focus on the strong ions. The cost for pH control was taken into account by the required concentration of pH-regulating acid and base. Further, we modeled the impact of pH on the growth by introducing an inhibition factor to the Monod kinetics. In the next step, the oxygen supply is examined in detail.

Oxygen supply via aeration and agitation

In aerobic fermentation, oxygen is a key component to the fermentation that may control the metabolism (Garcia-Ochoa et al., 2010). Due to its low solubility in water, oxygen has to be supplied continuously to the fermentation culture and its uniform distribution is a challenge of bioreactor design and scale-up (Garcia-Ochoa and Gomez, 2009; Clarke, 2013; Liu, 2020). In this work, we assumed an ideal mixture of the fermentation culture. The supply of oxygen was modeled via compressed air through a sparger and the distribution of oxygen via stirring (Porto de Souza Vandenberghe et al., 2022). For modeling the required electrical power, we considered the compression of air for aeration and the mixing for agitation.

The mass balance for dissolved oxygen in the fermentation culture reads

$$\frac{\mathrm{d}c_{O_2}}{\mathrm{d}t} = OTR - OUR = 0, \tag{20}$$

where OTR is the Oxygen Transfer Rate and OUR is the Oxygen Uptake Rate. We assumed a pseudo-steady state of the oxygen transfer, as it is practiced by other modeling examples, for example, Humbird et al. (2017). This assumption results in $\frac{\mathrm{d}c_{O_2}}{\mathrm{d}t} = 0$, from which follows $OUR = OTR$.

The OUR was calculated directly by its correlation with the oxygen uptake flux v_{O_2} in Eq. (21), based on the definition of OUR (Liu, 2020; Garcia-Ochoa et al., 2011). By directly using the oxygen uptake flux, we replaced a parameter of the bioreactor level, namely, the respiration rate, with a variable from the cellular level, which is v_{O_2}. Thus, the predictions at the bioreactor level profit from the accuracy of the GEM. In Eq. (22), we assumed that the provided oxygen gas stream equals the volume flow of oxygen taken up. We assumed air to be an ideal gas,

with a volumetric composition of 21% oxygen (see Eq. (23)).

$$OUR = v_{O_2} M_{O_2} c_{bio} \tag{21}$$

$$\dot{V}_{O_2} = \frac{OUR \cdot V_{culture}}{\rho_{O_2}} \tag{22}$$

$$\dot{V}_{air} = \frac{\dot{V}_{O_2}}{0.21}. \tag{23}$$

As it is common practice, based on the two-film theory, the resistance in the liquid boundary layer of the gas–liquid interface was assumed to be decisive for the OTR (Clarke, 2013; Seidel et al., 2021). Hence, the resistances in the gaseous boundary layer and the boundary layer at the cell membrane were omitted (Eq. (24)). The $k_L a$-value was then calculated using the van't Riet correlation (Van't Riet, 1979) for a non-coalescing medium in Eq. (25). The power of agitation is taken into consideration through this equation. Further, we ignored the influence of aeration on power input because this depends on specific bioreactor design decisions, e.g., type and amount of agitators. In Eq. (26), the superficial gas velocity was calculated based on the assumption of a cylindrical reactor (Eq. (27)).

$$OTR = k_L a \left(c_{O_2,equil} - c_{O_2} \right) = k_L a \cdot (1 - \varphi) \cdot c_{O_2,equil} \tag{24}$$

$$k_L a = 0.002 \left(\frac{P_{agitation}}{V_{culture}} \right)^{0.7} u_s^{0.2} \tag{25}$$

$$u_s = \frac{\dot{V}_{air}}{A_{cross}} \tag{26}$$

$$A_{cross} = \frac{\pi}{4} D^2, \tag{27}$$

where $k_L a$ is a lumped parameter for overall volumetric oxygen transfer. The concentration c_{O_2} refers to the oxygen concentration in the fermentation culture (also called dissolved oxygen), whereas $c_{O_2,equil}$ denotes the oxygen concentration at the gas–liquid interface, i.e., the solubility of oxygen in the fermentation culture when assuming chemical equilibrium at the interface. The parameter φ correlates oxygen concentration in the culture with oxygen solubility. In Eq. (24), we set $c_{O_2} = \varphi \cdot c_{O_2,equil}$ with $\varphi = 0.3$ (Bernard and Payton, 2001; Strandberg et al., 1991) to avoid oxygen limitation of the fermentation, which can occur already at low dissolved oxygen levels (Hansen et al., 2022). Further, u_S denotes the superficial gas velocity. The cross-sectional area of the fermentation culture A_{cross} equals the base surface of the fermentation culture.

With the superficial gas velocity and the agitation power at hand, the gas holdup can be calculated. The gas holdup specifies the dispersed gas in an aerated bioreactor. It becomes more and more important with increasing bioreactor sizes and commonly lies between 10 and 30% (Villadsen et al., 2011; Nienow, 2009). The gas holdup can be correlated to the superficial gas velocity and the specific agitation power input (Sieblist and Lübbert, 2010; Yawalkar et al., 2002; Bailey and Ollis, 1986) and was calculated in Eq. (28), based on the correlation of Weißgärber (1976). The gas holdup volume was calculated using the definition of the gas holdup in Eq. (29).

$$\epsilon_{gas} = 1.12 \cdot \left(\frac{P_{agitation}}{V_{culture} \cdot \rho_{culture}} \right)^{0.29} \cdot u_S^{0.6} \tag{28}$$

$$\epsilon_{gas} = \frac{V_{gas}}{V_{gas} + V_{culture}}, \tag{29}$$

where ϵ_{gas} stands for the gas holdup. The culture density was approximated with the density of water (Mayer et al., 2023; Martínez-Salas et al., 1981).

The required power for aeration was calculated by the thermodynamic equation of adiabatic, isentropic compression of ideal gases (Biegler, 1997; Ulonska et al., 2016; Cardoso et al., 2020) in Eq. (30).

We assumed the feedstock cost of air to be small compared to compressor cost and cost for power, which is why we neglected them.

$$\begin{aligned} P_{compress} &= \dot{n}_{air} \frac{1}{\eta_{compress}} \frac{\alpha}{\alpha - 1} RT \left(\left(\frac{p_{air}}{p^0} \right)^{\frac{\alpha-1}{\alpha}} - 1 \right) \\ &= p^0 \dot{V}_{air} \frac{1}{\eta_{compress}} \frac{\alpha}{\alpha - 1} \left(\left(\frac{p_{air}}{p^0} \right)^{\frac{\alpha-1}{\alpha}} - 1 \right), \end{aligned} \tag{30}$$

where $\dot{n}$ denotes the mole flow rate; η is an efficiency number, α is a polytropic exponent. The ideal gas constant R and the temperature T cancel each other out when applying the ideal gas law $p^0 \dot{V}_{air} = \dot{n}_{air} RT$. Atmospheric pressure is denoted with p^0. The chosen values for the parameters $\eta_{compress}$, α, and p_{air} are tabulated in Table A.2. Note that p_{air} was set to 2.5 bar.

In summary, aeration was modeled by setting the oxygen uptake at the cellular level about the required oxygen supply and the oxygen transfer rate. The oxygen transfer rate is decisive for the required agitation power. The cost of aeration was calculated by taking into account the capital cost of the compressor and the required power for compression. The next and last modeling aspect is an energy balance including cooling.

Cooling

In aerobic fermentation, cooling is an important aspect of bioreactor design, since temperature affects the microbial metabolism and the oxygen solubility (Clarke, 2013). Especially for large bioreactors, providing enough heat transfer surface is crucial, since the ratio of surface area to reactor volume decreases with increasing reactor size (Clarke, 2013). Heat is mainly transferred from the metabolic activity and the agitation (Rao et al., 2006), as depicted in Eq. (31), with the agitation heat equaling the agitation power input (Knoll et al., 2005) in Eq. (32). Again, we ignored the influence of aeration on power input.

$$\dot{Q} = \dot{Q}_{agitation} + \dot{Q}_{met} \tag{31}$$

$$\dot{Q}_{agitation} = P_{agitation}, \tag{32}$$

where $\dot{Q}$ denotes the heat flow; and the subscript *met* stands for metabolic.

In bioreactor design, it is common to correlate metabolic heat with the OUR or the OTR (Doran, 1995; Knoll et al., 2005; Cooney et al., 1969). We applied the correlation

$$\dot{Q}_{met} = \delta \cdot \frac{OUR \cdot V_{culture}}{M_{O_2}}, \tag{33}$$

where the correlation parameter $\delta = 0.13\,\mathrm{kW\,h\,mol^{-1}}$ is a mean value of the values specified in the aforementioned publications.

We assumed that the temperature of the fermentation culture is known, constant in time, and uniform in space. The heat transfer through the cooling agent was modeled in Eq. (34). The required power for pumping the cooling agent through the cooling coil was calculated similarly to Knoll et al. (2005) in Eq. (35).

$$\dot{Q} = \dot{m}_{cooling} \cdot c_{p,heat} (T^{in}_{cooling} - T^{out}_{cooling}) \tag{34}$$

$$P_{cooling} = \frac{\dot{m}_{cooling} \cdot g \cdot (H_{culture} + H_{gas})}{\eta_{pump}}, \tag{35}$$

where $c_{p,heat}$ is the specific heat capacity of the cooling agent at the mean temperature of the cooling agent T_{mean} and g denotes gravity. We chose cooling water as the cooling agent at input temperature $T^{in}_{cooling} = 15\,^\circ\mathrm{C}$. The final temperature of the cooling water $T^{out}_{cooling}$ was assumed to be 25 °C, which was 5 °C below the temperature of the fermentation culture $T_{culture}$ (Heinzle et al., 2006). The mean temperature was calculated by the logarithmic mean temperature difference, i.e., $T_{mean} = 20.9\,^\circ\mathrm{C}$.

Table 1
Comparison between the formulations SimulKnock and the extension SimulKnockReactor of this work. UL: upper level, LL: lower level, FBA: flux balance analysis, conc.: concentration, KO's: knockouts.

Aspect	SimulKnock	This work: SimulKnockReactor
Optimization class	Bilevel (UL & LL)	Bilevel (UL & LL)
Input parameters	Metabolic network, maximum number of KO's	Metabolic network, maximum number of KO's, production capacity
Implemented kinetics	Monod or Michaelis–Menten	Monod with pH-inhibition
Upper Level (UL)	Fermentation	Fermentation & bioreactor
Objective function	Space–time yield	Bioreactor cost
Modeled compounds	Substrate, product, biomass	Substrate, product, biomass, oxygen, hydrogen, strong ions
Degrees of freedom	Knockout variable, substrate feed conc.	Knockout variable, substrate feed conc., conc. pH control agents, agitation power, compression power, mass flow cooling agent, optional: number of parallel reactors
Additional variables	Growth/ dilution rate	Growth/ dilution rate, height and diameter of fermentation culture, volume of reactor, compression of air, agitation, cooling, pH control
Lower Level (LL)	FBA	FBA
Objective function	Growth rate	Growth rate
Degrees of freedom	Metabolic fluxes	Metabolic fluxes

2.3. SimulKnockReactor: Combined optimization formulation

We combined the formulation of SimulKnock with the equations from bioreactor design and cost analysis. The combined optimization formulation SimulKnockReactor reads:

min cost

s.t. cost calculation (Eq. (7)),
investment cost reactor and compressor (Eqs. (8)–(9)),
bioreactor sizing (Eqs. (10)–(14) and (28)–(29)),
pH control (Eqs. (16)–(17)),
growth inhibition through pH (Eqs. (18)–(19)),
oxygen uptake and transfer (Eqs. (20)–(24)),
power for agitation & compression (Eqs. (25)–(27) and (30)),
energy balance and heat transfer (Eqs. (31)–(34)),
pumping power for cooling (Eq. (35)),
mass balances fermentation & number of knockouts (Eqs. (2)–(4)),

max growth rate

s.t. mass balances & knockout constraints (Eqs. (6)).

The difference to SimulKnock lies in the upper-level program: it includes bioreactor design aspects now. Thus, the objective function is different. The number of modeled compounds and the degrees of freedom have increased. A detailed comparison between SimulKnock and this work's extension, SimulKnockReactor, is depicted in Table 1.

2.4. Implementation

For implementation and solution, we reformulated the bilevel program to a single-level program using strong duality. This is a standard technique also used in OptKnock (Burgard et al., 2003) and in SimulKnock (Ziegler et al., 2024), which comes at the expense of an increased number of variables due to the introduction of so-called dual variables. The resulting optimization program is a mixed-integer nonlinear optimization program. Similar to SimulKnock, we used auxiliary variables to reformulate the nonlinear constraints of the substrate mass balance with Monod kinetics (Eq. (3)) and the CPM model ((19)) such that they could be solved by commercial solvers, e.g., Gurobi (Gurobi Optimization, 2023). The remaining nonlinear functions, i.e., the investment cost calculation of the reactor (Eq. (8)) and the compressor (Eq. (9)), the definition of pH (Eq. (16)), the van't Riet correlation of the $k_L a$-value (Eq. (25)), and the gas holdup correlation (Eq. (28)) are treated through dynamic outer approximations as part of the branch and bound tree. To achieve this, we used so-called general constraint functions from Gurobi (Gurobi Optimization, 2023). The reformulated optimization formulation was implemented with the software Pyomo (Hart et al., 2011; Bynum et al., 2021) and solved with Gurobi v11.0.3 (Gurobi Optimization, 2023), using the preprocessing procedure of SimulKnock (Ziegler et al., 2024).

3. Case studies

In the following, we show the applicability and the mode of action of SimulKnockReactor in exemplary case studies. We applied SimulKnockReactor for the production of three different target chemicals: formate, acetate, and succinate. We chose the well-examined *E. coli* K12 as an exemplary organism and embedded two different metabolic networks of the organism: the *E. coli* core network (Orth et al., 2010a) and the GEM *i*ML1515 (Monk et al., 2017). The optimization problem with the embedded GEM (single-level reformulation) is numerically very challenging, due to the large number of variables (around 1.3×10^4 continuous variables, 2.7×10^3 binary variables, and one integer variable), the large number of constraints (1.5×10^4), and the nonlinearity (7 nonlinear equality constraints). For all optimization runs, we limited the runtime to 10 h on 48 cores. When the optimization does not converge to a global solution within this runtime, we read out the local solution. We only reported available solutions and further discriminated against solutions having a higher objective value than the core network solution. The solution with the embedded core network

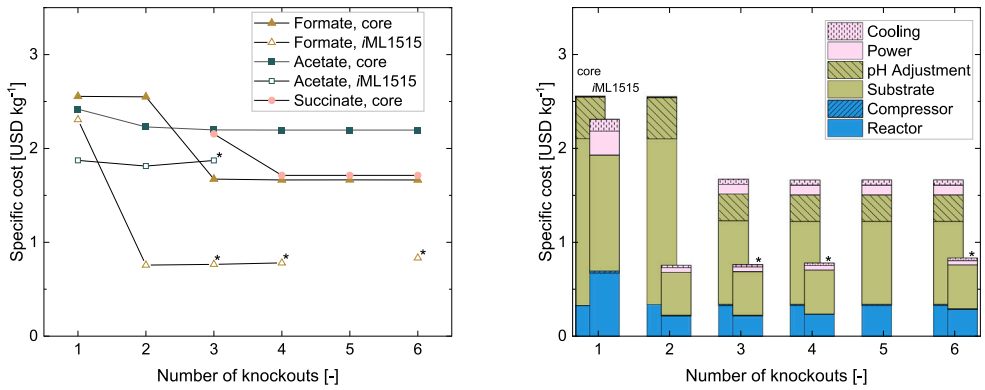

(a) Total cost (b) Formate: cost factors

Fig. 3. Influence of the maximum allowable number of knockouts on the specific production cost. The production capacity was set to $10^3\,\mathrm{kg\,a^{-1}}$. The asterisk * indicates locally optimal solutions; all other solution points are globally optimal. The embedded networks are *E. coli* core (Orth et al., 2010a) (indicated or bars in the back) and *i*ML1515 (Monk et al., 2017) (indicated or bars in the front) USD: US-Dollar. (a) Total cost for acetate, succinate, and formate, (b) Formate production cost divided into the individual cost factors. Blue, green, and pink color denotes investment cost, raw materials, and utilities, respectively.

is supposed to be worse since the core network has fewer reaction pathways included. In general, the local solution is an upper bound of the global solution; hence, better solutions might exist.

In the following, we examined the influence of the number of knockouts and the production capacity on the total cost and the individual cost factors. Moreover, we compared our simultaneous approach with a sequential approach and to a thermochemical formate production process from industry.

In all cases, substrate uptake reaches its upper bound of $10\,\mathrm{mmol\,g_{CDW}^{-1}\,h^{-1}}$, which was to be expected due to the structure of the SimulKnockReactor framework and the implemented Monod kinetics.

3.1. Decreasing cost with an increasing number of knockouts

In this case study, we increased the total number of maximum allowable number of knockouts from one to six. The total specific cost for formate, acetate, and succinate are depicted in Fig. 3(a).

The total cost decreases with an increasing number of knockouts. The slight increase in cost for acetate and formate production with the embedded GEM can be explained by the fact that solutions responsible for the rise are only local optima. A lower (globally optimal) solution value most likely exists. For succinate production, the optimization software, that is, the solver, only returns a feasible solution for three knockouts or more. For succinate production with the embedded GEM, the solver did not return any global or local solution.

For each target product, there is a plateau at which a further increase in the number of knockouts does not reduce costs any further or only insignificantly. For example, this plateau is reached for succinate production at four knockouts and for formate production with the embedded GEM at two knockouts.

Where a solution is available, the costs with the embedded GEM are lower than the costs with the embedded core network. For one maximum allowable knockout, the predicted knockout for acetate production with the embedded core network and the GEM is similar, namely ATP synthase. Presumably, the GEM includes a more efficient pathway towards biomass, which can explain the better objective value with the embedded GEM despite the same knockout strategy. The predicted knockout for formate production is NADH dehydrogenase with embedded core network and ATP synthase with embedded GEM. The fact that the knockout for formate and acetate production is the same with embedded GEM illustrates the optimistic nature of SimulKnockReactor. Competing metabolic pathways are not taken into account in the formulation.

For two maximum allowable knockouts, the predicted knockouts with the embedded GEM and core network differ for acetate and formate production. In formate production with the embedded GEM, for example, the knockout of ATP synthase and glutamate dehydrogenase results in a drastic cost decrease. For comparison, predicted knockouts with the embedded core network are glutamate dehydrogenase and NADH dehydrogenase. Hence, differing knockout predictions are a second explanation for different objective values. Moreover, with the embedded GEM, the plateau is reached earlier. For example, acetate costs stagnate after one knockout with the embedded GEM, while they reach a plateau only after two knockouts with the embedded core network. This could also be due to the decreased pathway options in the core network.

Exemplarily, Fig. 3(b) depicts the individual cost factors for formate production. Not surprisingly, the biggest cost driver is substrate cost, amounting to 53 to 69% of the total cost. For these small production capacities, 50% is a typical value. Further, the pH adjustment agent is a non-negligible factor, which matches the findings of Saur et al. (2023) in their techno-economic analysis of itaconic acid production. Substrate costs are followed by investment costs, which consist almost entirely of reactor costs. The compressor investment cost, and also compressor power costs, are low due to the small reactor size. Utilities are the lowest cost item, split roughly equally between power and cooling costs. This cost distribution is also observable for acetate and succinate production (see Fig. A.1).

If one compares the results with the embedded core network with those with the embedded GEM, the shares are different. For example, the pH adjusting agent is not a cost factor with the embedded GEM, in contrast to results with the embedded core network. Presumably, the GEM allows for intracellular pH adjustment. Another example of different cost allocations is formate production with one knockout (which is ATP synthase with GEM and NADH dehydrogenase with core network embedded). The predicted process with the embedded core network operates with one reactor, $0.015\,\mathrm{m^3}$, an oxygen mole flow of $0.21\,\mathrm{mol\,h^{-1}}$ (that is, $0.016\,\mathrm{mol\,L^{-1}\,h^{-1}}$), a specific power input of $0.53\,\mathrm{kW\,m^{-3}}$ and a pH of 7.1. On the other hand, the process with the embedded GEM operates with one reactor of $0.05\,\mathrm{m^3}$, an oxygen mole flow of $5.9\,\mathrm{mol\,h^{-1}}$ (that is, $0.18\,\mathrm{mol\,L^{-1}\,h^{-1}}$), a specific power input of $5.9\,\mathrm{kW\,m^{-3}}$ and a pH of 6.5. Note that the results with embedded GEM show pH values equal or less than 6.5 or equal or greater than 7.5 due

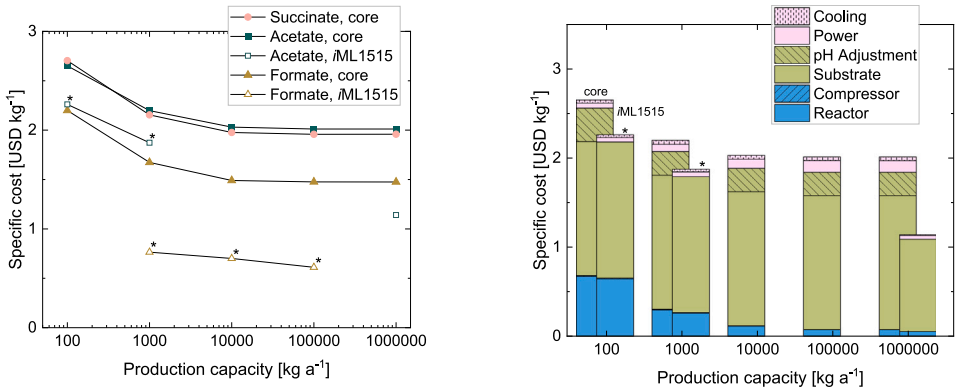

(a) Total cost (b) Acetate: cost factors

Fig. 4. Influence of the production capacity on the specific production cost. The maximum allowable number of knockouts is set to 3. The asterisk * indicates locally optimal solutions; all other solution points are globally optimal. The embedded networks are *E. coli* core (Orth et al., 2010a) (indicated or bars in the back) and *i*ML1515 (Monk et al., 2017) (indicated or bars in the front). USD: US-Dollar. (a) Total cost for acetate, succinate, and formate, (b) Acetate production cost divided into the individual cost factors. Blue, green, and pink color denotes investment cost, raw materials, and utilities, respectively.

to an initial setting—with negligible effect on the results. This example shows that the optimal operation point may differ depending on the chosen metabolic network.

3.2. Economies of scale come into play when the production capacity is increased

In the next case study, we varied the production capacity from $100\,\mathrm{kg\,a^{-1}}$ to $10^6\,\mathrm{kg\,a^{-1}}$ and examined the impact of this variation on the total specific cost and the individual cost factors. Fig. 4(a) depicts the total specific cost for succinate, acetate, and formate production. With the embedded GEM, no global or local solution was found for succinate production. Furthermore, the local solution for formate production of $100\,\mathrm{kg\,a^{-1}}$ was higher than the result with the embedded core network and therefore excluded from the figure.

Economies of scale apply to acetate production (see Fig. 4(b)), that is, the larger the production capacity, the smaller the specific cost (for formate and succinate cost factors, see Fig. A.2). With the embedded core network, total cost decreases by 24% from 100 to $10^6\,\mathrm{kg\,a^{-1}}$; with the embedded GEM, the decrease is 50% from 100 to $10^6\,\mathrm{kg\,a^{-1}}$. Especially the reactor investment cost decreases with increasing production capacity (see Fig. 4(b)). Moreover, again, no pH adjustment is predicted with the embedded GEM. The knockout strategy with the embedded core network remains the same across the entire range of production capacity. As shown in Section 3.1, two knockouts are sufficient to reach a cost plateau for acetate production, namely ATP synthase and pyruvate kinase. Hence, the third chosen knockout has little effect. For $10^6\,\mathrm{kg\,a^{-1}}$ acetate production with the embedded GEM, the suggested knockouts are also ATP synthase and pyruvate kinase. The other cases with the embedded GEM predict other knockout targets next to ATP synthase, however, these knockouts have little effect, as argued in Section 3.1. Overall, we concluded that economies of scale apply. However, they only apply to investment costs (see (8) and (9)). With substrate cost being the largest cost factor, however, they do not change the orders of magnitude. Considering economies of scale also in the procurement of raw materials might change the picture.

3.3. The simultaneous approach outperforms a sequential approach

Our scientific hypothesis is that simultaneous optimization is advantageous over sequential optimization for microbe and bioreactor design. In order to examine the validity of this hypothesis, we defined a sequential approach with two steps. In the first step, OptKnock (Burgard et al., 2003) predicts knockouts for a specified target product and a fixed maximum allowable number of knockouts. The predicted knockouts are handed over to a second step. In the second step, SimulKnockReactor minimizes the reactor cost for the specified target product with fixed knockouts. Note that already this approach is itself a novelty. This two-step procedure reflects the established approach to first optimize the microorganism and then design the bioreactor.

We applied this sequential approach to formate, acetate, and succinate production with an embedded *E. coli* core network (Orth et al., 2010a). We chose to work with the core network to gain a full overview of the cases and have less impact by numerical issues. The production capacity was set to $10^3\,\mathrm{kg\,a^{-1}}$ to make the results directly comparable with the results from Section 3.1 (with embedded core network).

When performing the sequential approach, different outcomes may arise for the different target products and number of knockouts. These outcomes are based on the feasibility of an optimization program. In general, an optimization program has a feasible solution if all equalities and inequalities are satisfied by one set of variables (Edgar et al., 2001). In coherence with this definition, the solver returns a statement of whether the optimization program has a feasible solution. Due to numerical reasons, however, this output may not reflect the mathematical truth; for example, the program may be infeasible even if the solver returns a solution. The case that the solver declares a program infeasible even if it is actually feasible, however, is unlikely in global optimization. Therefore, we reported feasibility based on the solver output.

In the different case studies, the solver may return that the sequential optimization program is infeasible in the first stage. However, we did not observe this outcome in our case studies. Next, the sequential optimization program can turn infeasible in the second stage. When this is the case, it is interesting to compare with the behavior using SimulKnockReactor. If the solver returns a feasible solution using SimulKnockReactor, this indicates that the proposed knockouts using OptKnock are not able to fulfill the production capacity requirements of the reactor stage, while the knockouts using SimulKnockReactor are. The case where the optimization program using the sequential approach has a feasible solution and the optimization program using the simultaneous approach is infeasible is mathematically not possible and numerically very unlikely because the solver is free to choose the same knockouts as OptKnock also with the simultaneous approach. When the solver returns a feasible solution with both approaches, we compared the proposed knockout strategy. From the same proposed knockouts, it follows directly that the objective values are the same, too. With different proposed knockouts, the objective value with SimulKnockReactor can be equally good or better than with the sequential

Table 2
Observed outcomes based on the solver output for formate, acetate, and succinate production from one to six knockouts and a production capacity of $10^3\,kg\,a^{-1}$ with the embedded *E. coli* core (Orth et al., 2010a) network.

Sequential \ SimulKnockReactor	feasible	infeasible
feasible	(A) same knockouts (B) different knockouts, same objective value (C) different knockouts, SimulKnockReactor better (not observed)	not observed
infeasible (2nd stage)	(D)	(E)

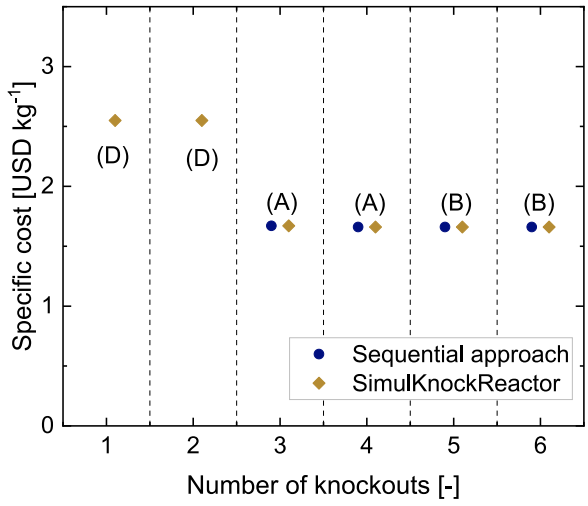

Fig. 5. Specific cost of formate over the number of knockouts for the sequential approach and SimulKnockReactor. Production capacity is set to $10^3\,kg\,a^{-1}$; the embedded network is *E. coli* core (Orth et al., 2010a). Outcomes A, B, and D are defined in Table 2. USD: US-Dollar.

approach. The case that the objective values with SimulKnockReactor are worse is mathematically not possible since the same knockouts as OptKnock can be chosen. Nevertheless, it can still happen with the solver because the simultaneous optimization program is numerically very challenging. The outcomes that we observed in our case studies are depicted in Table 2. Exemplarily, Fig. 5 shows the specific cost of formate production; the data for acetate and succinate can be found in the Supplementary Information.

The solver returns feasible solutions in more cases with SimulKnockReactor than with the sequential approach (outcome D). Example cases for this outcome are formate production with one and two knockouts (see Fig. 5) and succinate production with more than three knockouts (below three knockouts, also SimulKnockReactor is infeasible). Hence, the optimization program of the sequential approach appears to be more prone to infeasibility when few knockouts are allowed.

For the cases where the solver returns feasible solutions with both approaches, SimulKnockReactor objective values are equally good than the ones of the sequential approach (outcomes A and B). The same knockouts (outcome A) are predicted for formate production with three and four knockouts. In tendency, the higher the maximum allowable number of knockouts, the more the predicted knockouts differ despite same objective values (outcome B). This can be explained by predicted knockouts that do not further improve the result, as is the case with formate production with five to six knockouts (see Fig. 5). Furthermore, with more knockouts allowed, the number of possible combinations that lead to the same objective value may increase.

SimulKnockReactor and OptKnock both couple growth with product formation. Strains with growth-coupled production generally produce reliably over time in the bioreactor, which could be one explanation for the good performance of the sequential approach. Moreover, the biggest cost item is substrate cost, with SimulKnockReactor and with the sequential approach. For commodity chemicals, this is a usual finding. The substrate flux, in turn, directly influences the product flux, which is the objective function of OptKnock. Hence, currently, there is a strong correlation between the simultaneous and the sequential approach due to carbon yield being the dominating factor. This correlation is expected to be less strong if other cost drivers become more important, for example, through raised electricity or compressor costs or by considering salt disposal from the pH adjusting agents.

3.4. Industrial, thermochemical formate production is still cheaper but of the same order of scale as biochemical production

In our last case study, we evaluated the production cost of formate with a production capacity of $2.71 \times 10^7\,kg\,a^{-1}$. We, thereby, aimed to compare the cost of the biochemical production of formate with the cost of an established thermochemical production route. Moreover, we wanted to evaluate the prediction ability of SimulKnockReactor in a real-world example. With a worldwide market share of 32.1% in 2013 and a company-specific production process (Hietala et al., 2003), the company BASF was chosen as a benchmark for thermochemical formate production. Production costs of the thermochemical formate production were taken from Da Cunha et al. (2018), who optimized the total annual cost of the formic acid process by the BASF company (Hietala et al., 2003) in a bi-objective optimization. Production costs of the biochemical route were predicted with SimulKnockReactor using local optimization. The production capacity was set to $2.71\times10^7\,kg\,a^{-1}$, equal to Da Cunha et al. (2018), and the number of possible knockouts was set to three. The prediction was performed using the *i*ML1515 network (Monk et al., 2017). In SimulKnockReactor, the reactors and the compressor amount to investment cost; substrate and pH adjusting agent sum up to raw materials; and power and cooling make up for utilities. Operating labor costs were not considered in SimulKnockReactor and are therefore not available. Fig. 6(a) depicts the production cost of formate in the BASF process and predicted by SimulKnockReactor.

Biochemical production is 60% more expensive than the thermochemical production. The biggest difference lies in the cost of raw materials. With SimulKnockReactor, the raw materials account for 76% of the total cost, which is on the upper end of a typical range with large production capacities. However, the value highly depends on the process and the product. In the large-scale production of itaconic acid, for example, Nieto et al. (2020) found that the raw materials only account for around 12% of total OPEX per year. While the BASF process is based on carbon monoxide ($0.07\,USD\,kg^{-1}$), methanol ($0.672\,USD\,kg^{-1}$), and water ($0.001\,USD\,kg^{-1}$) (Da Cunha et al., 2018), the main substrate of the biochemical route is the more expensive glucose ($0.79\,USD\,kg^{-1}$) (ChemAnalyst, 2023b). Adjusting agents for pH are not needed and, thus, their costs are zero. The BASF process includes recycling streams, which increase the product yield. Recycling streams were not considered in the biochemical process (see Fig. 6(b)). The outlet stream only contains low substrate concentrations ($0.03\,g\,L^{-1}$), so substrate recycling is not of interest. However, recycling or retention of biomass could be interesting to decouple growth from the dilution rate and achieve lower residence times. Moreover, an increased yield would be more favorable. Currently, the yield of formate per substrate on a carbon molar basis is 56%. However, the main side product is biomass, which is also needed for production.

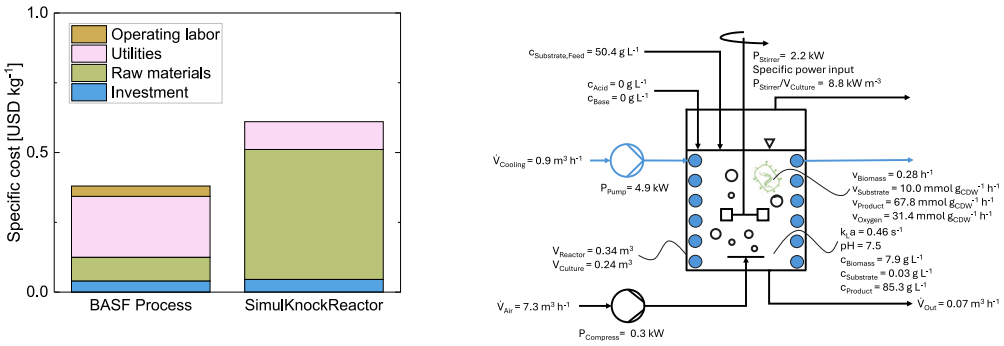

(a) Cost factors (b) Predicted bioreactor and microbe design

Fig. 6. Comparison of an optimized thermochemical production process from BASF (Da Cunha et al., 2018; Hietala et al., 2003) and the biochemical production predicted with SimulKnockReactor. The production capacity is $2.71 \times 10^7\,\mathrm{kg\,a^{-1}}$. SimulKnockReactor is run for three maximum allowable knockouts with the embedded genome-scale metabolic model *i*ML1515 (Monk et al., 2017). USD: US-Dollar, c: concentration, P: power, V: volume. (a) Distribution of formate production costs (b) Bioreactor and microbe design variables predicted using SimulKnockReactor. With the embedded GEM, the pH value can only take values less than or equal to 6.5 or greater than or equal to 7.5 due to an initial setting. The exclusion of this region has a negligible impact on the results.

The utility costs are the largest cost factor in the BASF process, presumably due to the high pressure and temperature levels required for the thermochemical reaction and separation. This finding highlights the advantage of biochemical processes, which run at moderate temperature and pressure levels. However, it should be noted that the BASF process includes separation units and heat integration, which are not considered in SimulKnockReactor. This mismatch makes a deepened comparison difficult.

The investment costs are similar in both processes. The biggest share with SimulKnockReactor is the reactor investment costs. Namely, in order to reach the production capacity, 545 reactors operate in parallel, with a volume of $0.34\,\mathrm{m^3}$ each. The solver only returns a single optimal point that satisfies the optimal objective value. However, other optimal solutions may exist. For example, if the metabolic network contains two pathways that are equally effective, the solver arbitrarily picks one. Analogously, it is possible that a solution with fewer, larger reactors exists which is just not returned by the solver. Another reason could be that smaller reactors actually achieve lower costs by the specific power input, which is bigger with smaller culture volumes. The specific power input directly influences the oxygen uptake (see (25)), which in turn is decisive for growth and product formation. The more realistic alternative of fewer reactors with larger volumes each is hence just not returned by the solver because this alternative furnishes equal objective values or it is not chosen by the solver due to higher specific power input in small reactors. Adaptation of the model by penalizing parallelization of reactors could potentially tackle this issue. This large amount of reactors is needed due to the large residence time, that is, 3.5 h. As a reminder, due to continuous fermentation conditions, the residence time is the inverse of the growth rate. Decreasing the residence time would, hence, only be possible by increasing the growth rate. In contrast, in the BASF process, the residence time in reactor 1 and 2 are 0.717 h and 0.202 h, respectively. Thus, the separation units presumably account for the largest share of investment cost.

Lastly, despite the mismatch discussed above, we want to point out that the costs of the BASF process and the biochemical process predicted with SimulKnockReactor range in the same order of scale, which demonstrates the applicability of SimulKnockReactor as an early-stage process evaluation tool.

4. Conclusion and outlook

We presented a bilevel optimization formulation, named SimulKnockReactor, which combines bioreactor design with microbial strain design. It is an extension of our previous work SimulKnock (Ziegler et al., 2024). The upper level minimizes total bioreactor costs and includes the mass and energy balances of the fermentation, as well as the dimensioning of the reactor, the aeration, the cooling, and the pH control. We referred to this level as bioreactor design, but excluded the selection of specific equipment, such as the type of stirrer. The lower level maximizes the growth of the microorganism and includes metabolite mass balances based on the metabolic model of the organism. We considered gene deletion as a genetic modification of the microbial strain. The bilevel optimization formulation was reformulated to a single-level program resulting in a mixed-integer nonlinear optimization program. It was solved using global and local optimization techniques.

Our results of the exemplary case studies with the *E. coli* core network (Orth et al., 2010a) and the GEM *i*ML1515 (Monk et al., 2017) showed that substrate cost was the biggest cost factor, which was in line with common knowledge on bioreactor costs. Further, we observed that the extent of pH adjustment cost depended on the embedded network. With an increasing number of knockouts, the production cost decreased until it reached a plateau. As production capacity increased, economies of scale occurred, especially in the investment costs for reactors. In comparison with a sequential approach, where OptKnock (Burgard et al., 2003) was applied and then the reactor cost was minimized, the solver returned feasible solutions in more case studies with SimulKnockReactor. This indicated that, with the knockouts predicted using OptKnock, the microorganism could not fulfill the requirements of the reactor stage, highlighting the techno-economic advantage of the simultaneous formulation.

We proved the solvability of SimulKnockReactor also for industrially relevant production capacities. However, the amount of reactors predicted by the solver was unrealistically high, presumably due to better oxygen distribution in small reactors. Additional constraints penalizing parallel operation could tackle this issue. To improve the accuracy of our aeration model, the employed van't Riet correlation to calculate the $k_L a$-value should be supported with experimental values or a strain-specific correlation could be employed. Furthermore, the hydrostatic pressure in the tank could be introduced as a variable. Taking into account the effects of aeration on agitation power input would further refine the modeling. The accuracy of the pH model could be increased by incorporating metabolic models including pH (Du et al., 2019), or by rigorous modeling of the pH, as suggested by Walz et al. (2017) and Brée et al. (2020). Concerning pH costs, it would be of interest to include downstream salt disposal costs, which can become a decisive

cost factor. Moreover, our assumption that genetic modifications do not influence the impact of pH on growth should be experimentally validated. The modeling of the cooling could be extended by considering the heat transfer surface of the cooling coils and a sensible upper bound on the mass flow of the cooling agent or pumping power.

Due to the mathematical structure of SimulKnockReactor with Monod kinetics, the substrate uptake was always at its upper bound, which, however, is not realistic. Substrate uptake is dependent on bioreactor conditions and metabolic modifications. Similar to as it was done in SimulKnock, by implementing Michaelis–Menten as an alternative kinetics, the substrate uptake could be influenced by the bioreactor conditions. However, it is expected that Michaelis–Menten kinetics further increase the numerical effort. In any case, analogous to SimulKnock, the assumption that the genetic modifications do not affect the kinetic parameters has to be tackled in the future.

Depending on the size of the metabolic network, the runtimes ranged from a few minutes using up to 8 threads (for core network) to several hours on 48 threads, with difficulties of convergence within the set time limit of 10 h (for GEM). To decrease computation times and tackle convergence issues, machine learning could be included to substitute the GEM, to include experimental data (e.g., on pH influence), or to learn nonlinear functions.

Beyond that, many, possibly modular extensions are conceivable. An extension could be the selection of specific devices for the bioreactor and the surrounding equipment in order to do full justice to the concept of bioreactor design. The inclusion of product inhibition, e.g., using a linear correlation of maximal growth with product concentration (Straathof, 2023), could be interesting. Furthermore, more aspects could be included, e.g., considerations about upstream and downstream units (Konstantinos and Kokossis, 2022; Tafur Rangel et al., 2022; Ploch et al., 2019; Cortes-Peña et al., 2020), as well as marketing and administration, transportation, and research and development, as indicated by Doran (1995), Liu (2020). Using multi-objective optimization, the global warming impact could be considered parallel to cost estimation, similar to the work of König et al. (2020).

In general, several solutions to the lower level program may exist (Bard, 1998; Dempe, 2002), which makes the solution of a bilevel program ambiguous (Mitsos et al., 2008). Our current optimistic formulation is one way to address this ambiguity. If there were several solutions for the lower-level program, the one that was best suited to the upper-level purpose was selected by the algorithm, which may have led to overly optimistic results. On the other hand, a pessimistic formulation would account for a non-cooperative, worst-case scenario. Namely, expanding the framework to a robust formulation similar to RobustKnock (Tepper and Shlomi, 2010) would take competing pathways into consideration. Moreover, due to the complexity of the metabolic network, several solutions with equally good objective values may exist, where one flux distribution is more realistic than the other. A screening method in which the previously found combination of knockouts is excluded and SimulKnockReactor is then run again could take this multiplicity of optimal solutions into account. At a more advanced level, multiplicity could be addressed by extending SimulKnockReactor with an approach considering multiple objectives of the lower level and ordering them hierarchically, based on the work of Akbari and Barton (2018).

The inclusion of co-feeding, up-regulation, and down-regulation of genes (Pharkya and Maranas, 2006), as well as dynamic operation (Mahadevan et al., 2002), i.e., batch and fed-batch, stay interesting. With increasing available computational power and similar to Klamt and Gilles (2004), the lower level could be replaced by elementary mode analysis (Schuster and Hiletag, 1994) that describes the microbe without specifying an artificial cellular objective. This replacement could also be an option to decouple product formation from growth. Especially for strains with decoupled product formation, bioreactor optimization is of great interest since these strains are not inherently stable in the bioreactor. A decoupling option could therefore enhance the importance of SimulKnockReactor further. In any case, finding and solving an example for a real design bottleneck is very desirable in the future.

Lastly, we want to emphasize again that, given the few publications that exist on model-based bioreactor design in general and bioreactor design coupled with the cellular level in particular, the presented formulation SimulKnockReactor can also enhance these fields of research. For example, it should be possible to run SimulKnockReactor without considering genetic modifications if the production of the target chemical is already growth-coupled. In this use case, the number of allowed knockouts would be set to zero. Presumably, the optimization of the reactor conditions will activate one path versus another at the cellular level, and, thus, refine the bioreactor optimization. For a quick, first approximation of bioreactor cost and size, the substrate concentration in the reactor could be set to zero such that pH and kinetics are not considered. We also want to highlight the usability of the sequential approach presented. Given the strong correlation between the knockouts predicted by SimulKnockReactor and OptKnock, the sequential approach has the major advantage of low runtime (programs with embedded GEM are solved on 8 cores within a few minutes). Even if all cellular variables at the upper level were replaced again by common correlations—making the lower level obsolete—SimulKnockReactor could contribute to establishing the term and field of optimal bioreactor design.

Nomenclature

Abbreviations

conc.	concentration
CPM	cardinal pH model
CSTR	continuous stirred-tank reactor
FBA	flux balance analysis
GEM	genome-scale metabolic model
OTR	oxygen transfer rate
OUR	oxygen uptake rate
substr.	substrate
USD	US-Dollar

Symbols

A	surface [m^2]
$\boldsymbol{B}$	mapping matrix [-]
c	concentration [$g\,L^{-1}$]
c_{bio}	biomass concentration [$g_{CDW}\,L^{-1}$]
c^{mol}	molar concentration [$mol\,L^{-1}$]
$c_{p,heat}$	specific heat capacity [$J\,kg^{-1}\,K$]
C	specific cost [USD kg^{-1} or USD m^{-3} or USD kWh^{-1} or USD h^{-1} or USD]
D	diameter [m]
f	fixed fraction [-]
g	gravity (9.81) [$m\,s^{-2}$]
H	height [m]
k	heat transfer coefficient [$W\,m^{-2}\,K^{-1}$]
k_La	volumetric oxygen mass transfer coefficient [s^{-1}]
K	dissociation constant [$mol\,L^{-1}$]
K_S	Monod constant [$g\,L^{-1}$]
m	mass [kg]
$\dot{m}$	mass flow [kg/h]
M	molar mass [$g\,mmol^{-1}$]
n_R	number of reactors set up in parallel [-]
$\dot{n}$	mole flow [$mol\,h^{-1}$]
OTR	oxygen transfer rate [$g\,L^{-1}\,h^{-1}$]
OUR	oxygen uptake rate [$g\,L^{-1}\,h^{-1}$]
p	pressure [Pa]
P	power input [kW]
pH	pH [-]

q	relation height to diameter [-]
$\dot{Q}$	heat flow [kW]
R	ideal gas constant (8.3145)[kJ kmol^{-1} K^{-1}]
$\boldsymbol{S}$	stoichiometric matrix [-]
t	operating time [h]
T	temperature [K]
u_s	superficial gas velocity [m s^{-1}]
v	flux [mmol g_{CDW}^{-1} h^{-1}]
v_{bio}	growth rate [h^{-1}]
V	volume [m^3]
$\dot{V}$	volume flow [m^3 h^{-1}]
y	knockout variable [-]
Greek letters	
α	polytropic exponent [-]
β	parameter that correlates reactor volume with culture volume [-]
γ	growth inhibition factor [-]
δ	parameter that correlates OUR with metabolic heat [kW h mol^{-1}]
ϵ	holdup [-]
η	efficiency number [-]
κ	maximum allowable number of knockouts [-]
ν	stoichiometric coefficient [-]
ρ	density [kg m^{-3}]
φ	parameter that correlates oxygen concentration with oxygen solubility [-]
Subscripts	
bio	biomass
CDW	cell dry weight
$compress$	compressor
$cross$	cross-sectional
$equil$	equilibrium
H^+	hydrogen ions
i	summation index
met	metabolic
O_2	oxygen
P	product
R	reactor
ref	reference
s	superficial
S	substrate
WT	wild-type
Superscripts	
m	number of metabolites
max	maximum
min	minimum
mol	molar
n	number of irreversible reactions
opt	optimal
r	number of (possibly reversible) reactions

CRediT authorship contribution statement

Anita L. Ziegler: Writing – original draft, Visualization, Validation, Software, Methodology, Investigation, Conceptualization. **Marc-Daniel Stumm:** Writing – review & editing, Validation, Software, Methodology, Investigation. **Tim Prömper:** Writing – review & editing, Visualization, Software, Methodology, Investigation. **Thomas Steimann:** Writing – review & editing, Methodology. **Jørgen Magnus:** Writing – review & editing, Methodology, Funding acquisition. **Alexander Mitsos:** Writing – review & editing, Supervision, Resources, Methodology, Funding acquisition, Conceptualization.

Funding

This project was funded by the Deutsche Forschungsgemeinschaft (DFG, German Research Foundation), Germany under Germany's Excellence Strategy – Cluster of Excellence 2186 "The Fuel Science Center" – ID: 390919832.

Declaration of competing interest

The authors have no conflict of interest.

Acknowledgments

Computations were performed with computing resources granted by RWTH Aachen University, Germany under project thes1557. We thank Luis Schrade and Ilias Ouzlim for their preliminary work on setting up the optimization formulation. We thank Clemens Kortmann for making the code compatible with the code framework of SimulKnock.

Appendix A

A.1. Tabulated metabolic and fermentation reaction parameters

Table A.1.

A.2. Tabulated bioreactor parameters

Table A.2.

A.3. Cost factors for acetate and succinate production over number of knockouts

Fig. A.1.

A.4. Cost factors for formate and succinate production over production capacity

Fig. A.2.

Appendix B. Supplementary data

Supplementary material related to this article can be found online at https://doi.org/10.1016/j.compchemeng.2025.109388.

Table A.1
Tabulated fermentation parameters, already presented and described in SimulKnock (Ziegler et al., 2024). Ref.: reference.

Symbol	Description	Value	Unit	Ref.
f	share of wild-type growth rate	0.1	–	–
K_S	Monod constant	0.044	g L^{-1}	Wick et al. (2001)
v_{ATP}^{lower}	ATP maintenance flux threshold	6.86	mmol g_{CDW}^{-1} h^{-1}	Monk et al. (2017)
v_{bio}^{max}	maximum growth rate	0.73	h^{-1}	Wick et al. (2001)
v_S^{upper}	upper bound substrate uptake	10	mmol g_{CDW}^{-1} h^{-1}	–

Table A.2
Tabulated bioreactor parameters.

Symbol	Description	Value	Unit	Reference
α	polytropic exponent	1.4	–	Luyben (2018)
β	headspace parameter	1.2	–	Van't Riet and Tramper (1991)
δ	metabolic heat correlation parameter	0.13	[kW h mol^{-1}]	Doran (1995), Knoll et al. (2005), Cooney et al. (1969)
$\eta_{compress}$	compressor efficiency	0.7	–	Cardoso et al. (2020)
η_{pump}	pump efficiency	0.7	–	–
$\rho_{cooling}$	cooling water density	1000	kg m^{-3}	–
$\rho_{culture}$	culture density	1000	kg m^{-3}	Mayer et al. (2023), Martínez-Salas et al. (1981)
ρ_{O_2}	oxygen density at $T_{culture}$	1.27	kg m^{-3}	Stephan et al. (2019)
φ	correlation parameter dissolved oxygen	0.3	–	Bernard and Payton (2001)
$c_{O_2,equil}$	oxygen solubility at $T_{culture}$	0.0068	g L^{-1}	Baburin et al. (1981), Vendruscolo et al. (2012)
$c_{p,heat}$	specific heat capacity cooling water at T_{mean}	4184	J kg^{-1} K^{-1}	Lemmon et al. (2024)
C_{acid}	sulfuric acid specific cost	0.064	USD kg^{-1}	ChemAnalyst (2024)
C_{base}	sodium hydroxide specific cost	0.29	USD kg^{-1}	ChemAnalyst (2023a)
$C_{cooling}$	specific cost cooling water	0.17	USD m^{-3}	Wang et al. (2021)
C_{Power}	power specific cost	0.06	USD kWh^{-1}	Humbird et al. (2017)
$C_{R,ref}$	reference reactor cost	40.000	USD	Powell and Hill (2008)
C_S	glucose specific cost	0.79	USD kg^{-1}	ChemAnalyst (2023b)
g	gravity	9.81	m s^{-2}	–
M_{acid}	molar mass sulfuric acid	98.1	g mol^{-1}	–
M_{base}	molar mass sodium hydroxide	40.0	g mol^{-1}	–
n_R^{upper}	maximum number of reactors in parallel	10	–	–
p^0	atmospheric pressure	1	bar	–
p_{air}	pressure of pressurized air	2.5	bar	Luyben (2018)
pH^{lower}	lower bound pH	4.5	–	Du et al. (2019)
pH^{max}	maximum pH	9	–	Rosso et al. (1995)
pH^{min}	minimum pH	4	–	Rosso et al. (1995)
pH^{opt}	optimum pH	7	–	Rosso et al. (1995)
pH^{upper}	upper bound pH	7.5	–	Akkermans et al. (2017)
q	relation height to diameter	2.5	–	Humbird et al. (2017)
R	ideal gas constant	8.3145	kJ kmol^{-1} K^{-1}	–
$t_{amortization}$	amortization period	15	a	Powell and Hill (2008)
t_{annual}	annual production hours	8400	h a^{-1}	Humbird et al. (2017)
$T_{culture}$	temperature fermentation culture	303.15	K	–
$T_{cooling}^{in}$	input temperature cooling water	288.15	K	–
$T_{cooling}^{out}$	output temperature cooling water	298.15	K	–
T_{mean}	mean temperature cooling water	293.15	K	–
v_{bio}^{opt}	maximum growth rate	0.73	h^{-1}	Wick et al. (2001)
$V_{R,ref}$	reference reactor volume	0.5	m^3	Powell and Hill (2008)
V_R^{upper}	upper bound on the reactor size	10	m^3	–

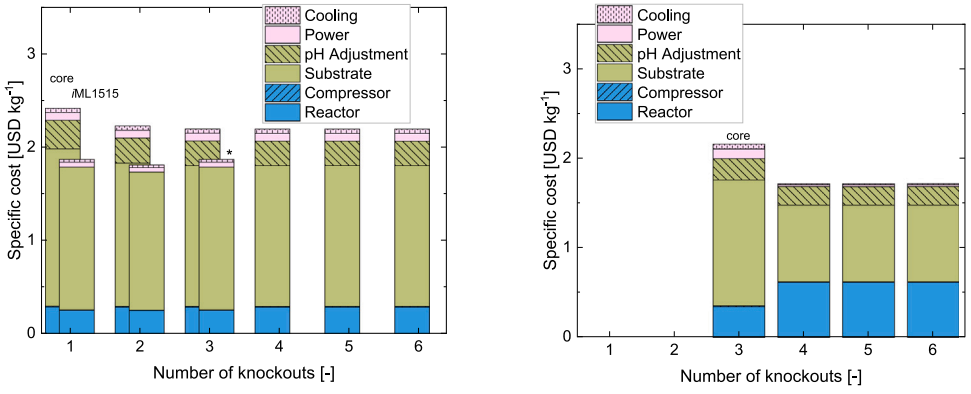

(a) Acetate: cost factors (b) Succinate: cost factors

Fig. A.1. Influence of the maximum allowable number of knockouts on the specific production cost. The production capacity was set to 10^3 kg a^{-1}. The asterisk * indicates locally optimal solutions; all other solution points are globally optimal. The embedded networks are *E. coli* core (Orth et al., 2010a) (indicated or bars in the back) and *i*ML1515 (Monk et al., 2017) (indicated or bars in the front) USD: US-Dollar. (a) Acetate and (b) succinate production cost divided into the individual cost factors. Blue, green, and pink color denotes investment cost, raw materials, and utilities, respectively.

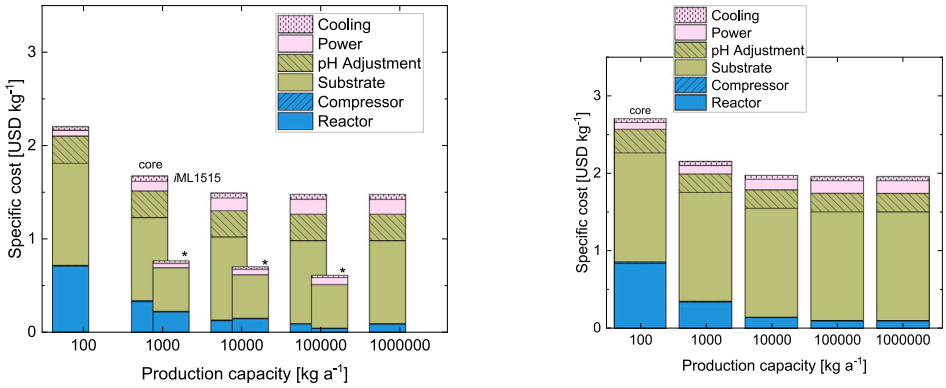

(a) Formate: cost factors

(b) Succinate: cost factors

Fig. A.2. Influence of the production capacity on the specific production cost. The maximum allowable number of knockouts was set to 3. The asterisk * indicates locally optimal solutions; all other solution points are globally optimal. The embedded networks are *E. coli* core (Orth et al., 2010a) (indicated or bars in the back) and *i*ML1515 (Monk et al., 2017) (indicated or bars in the front) USD: US-Dollar. (a) Formate and (b) succinate production cost divided into the individual cost factors. Blue, green, and pink color denotes investment cost, raw materials, and utilities, respectively.

Data availability

The implementation of the optimization formulation, the data preprocessing, and the interface with the solver Gurobi are openly available in our GitLab repository at https://git.rwth-aachen.de/avt-svt/public/simulknock.

References

Akbari, A., Barton, P.I., 2018. An improved multi-parametric programming algorithm for flux balance analysis of metabolic networks. J. Optim. Theory Appl. 178, 502–537. http://dx.doi.org/10.1007/s10957-018-1281-x.

Akkermans, S., Fernandez, E.Noriega., Logist, F., van Impe, J.F., 2017. Introducing a novel interaction model structure for the combined effect of temperature and pH on the microbial growth rate. Int. J. Food Microbiol. 240, 85–96. http://dx.doi.org/10.1016/j.ijfoodmicro.2016.06.011.

Baburin, L.A., Shvinka, J.E., Viesturs, U.E., 1981. Equilibrium oxygen concentration in fermentation fluids. Eur. J. Appl. Microbiol. Biotechnol. 13, 15–18. http://dx.doi.org/10.1007/BF00505335.

Bailey, J.E., Ollis, D.F., 1986. Biochemical Engineering Fundamentals, second ed. In: McGraw-Hill Chemical Engineering Series, McGraw-Hill, New York.

Bard, J.F., 1998. Practical Bilevel Optimization: Algorithms and Applications. In: Nonconvex Optimization and Its Applications, vol. 30, Springer, Boston, MA, http://dx.doi.org/10.1007/978-1-4757-2836-1.

Bernard, A., Payton, M., 2001. Fermentation and growth of Escherichia coli for optimal protein production. Curr. Protoc. Protein Sci. 5 (5.3), http://dx.doi.org/10.1002/0471140864.ps0503s00.

Bhonsale, S., Mores, W., van Impe, J., 2022. Nonlinear model predictive control based on multi-scale models: is it worth the complexity? IFAC-PapersOnLine 55, 129–134. http://dx.doi.org/10.1016/j.ifacol.2023.01.028.

Biegler, L.T., 1997. Systematic Methods of Chemical Process Design. In: Prentice Hall International Series in the Physical and Chemical Engineering Sciences, Prentice Hall PTR, Upper Saddle River, N.J.

Brée, L.C., Wessling, M., Mitsos, A., 2020. Modular modeling of electrochemical reactors: Comparison of CO2-electolyzers. Comput. Chem. Eng. 139, 106890. http://dx.doi.org/10.1016/j.compchemeng.2020.106890.

Burgard, A.P., Pharkya, P., Maranas, C.D., 2003. Optknock: a bilevel programming framework for identifying gene knockout strategies for microbial strain optimization. Biotechnol. Bioeng 84, 647–657. http://dx.doi.org/10.1002/bit.10803.

Bynum, M.L., Hackebeil, G.A., Hart, W.E., Laird, C.D., Nicholson, B.L., Siirola, J.D., Watson, J.P., Woodruff, D.L., 2021. third ed. Pyomo–optimization Modeling in Python, vol. 67, Springer Science & Business Media.

Campos, E., Flotats, X., 2003. Dynamic simulation of pH in anaerobic processes. Appl. Biochem. Biotechnol. 109, 63–76. http://dx.doi.org/10.1385/ABAB:109:1-3:63.

Cardoso, V.M., Campani, G., Santos, M.P., Silva, G.G., Pires, M.C., Gonçalves, V.M., de C Giordano, R., Sargo, C.R., Horta, A.C.L., Zangirolami, T.C., 2020. Cost analysis based on bioreactor cultivation conditions: Production of a soluble recombinant protein using Escherichia coli bl21(de3). Biotechnol. Rep. (Amst) 26, e00441. http://dx.doi.org/10.1016/j.btre.2020.e00441.

Chang, L., Liu, X., Henson, M.A., 2016. Nonlinear model predictive control of fed-batch fermentations using dynamic flux balance models. J. Process. Contr 42, 137–149. http://dx.doi.org/10.1016/j.jprocont.2016.04.012.

ChemAnalyst, 2023a. Caustic soda price trend and forecast: For the quarter ending september 2023; North America. URL https://www.chemanalyst.com/Pricing-data/caustic-soda-3. (Accessed 15 October 2023).

ChemAnalyst, 2023b. Dextrose price trend and forecast: For the quarter ending september 2023; North America. URL https://www.chemanalyst.com/Pricing-data/dextrose-1391. (Accessed 15 October 2023).

ChemAnalyst, 2024. Sulphuric acid price trend and forecast: For the quarter ending march 2024; north america. URL https://www.chemanalyst.com/Pricing-data/sulphuric-acid-70. (Accessed 24 July 2024).

Chmiel, H., Takors, R., Weuster-Botz, D. (Eds.), 2018. Bioprozesstechnik, forth ed. Springer Spektrum, Berlin and Heidelberg, http://dx.doi.org/10.1007/978-3-662-54042-8.

Clarke, K.G., 2013. In: Clarke, K.G. (Ed.), Bioprocess Scale Up. In: Bioprocess engineering, Woodhead Pub. Ltd, Cambridge, UK, pp. 171–188. http://dx.doi.org/10.1533/9781782421689.171.

Cooney, C.L., Wang, D.I., Mateles, R.I., 1969. Measurement of heat evolution and correlation with oxygen consumption during microbial growth. Biotechnol. Bioeng 11, 269–281. http://dx.doi.org/10.1002/bit.260110302.

Cortes-Peña, Y., Kumar, D., Singh, V., Guest, J.S., 2020. Biosteam: A fast and flexible platform for the design, simulation, and techno-economic analysis of biorefineries under uncertainty. ACS Sustain. Chem. Eng. 8, 3302–3310. http://dx.doi.org/10.1021/acssuschemeng.9b07040.

Da Cunha, S., Rangaiah, G.P., Hidajat, K., 2018. Design, optimization, and retrofit of the formic acid process I: Base case design and dividing-wall column retrofit. Ind. Eng. Chem. Res. 57, 9554–9570. http://dx.doi.org/10.1021/acs.iecr.8b00883.

de Oliveira, R.D., Guedes, M.N., Matias, J., Le Roux, G.A.C., 2021. Nonlinear predictive control of a bioreactor by surrogate model approximation of flux balance analysis. Ind. Eng. Chem. Res. 60, 14464–14475. http://dx.doi.org/10.1021/acs.iecr.1c01242.

Dempe, S., 2002. Foundations of Bilevel Programming. In: Nonconvex Optimization and Its Applications, vol. 61, Kluwer Academic, Dordrecht and Boston, http://dx.doi.org/10.1007/b101970.

Doran, P.M., 1995. Reactor engineering. In: Doran, P.M. (Ed.), Bioprocess Engineering Principles. Academic Press, London, pp. 333–391. http://dx.doi.org/10.1016/B978-012220855-3/50013-4.

Douglas, J.M., 1988. Conceptual Design of Chemical Processes, repr ed. In: Chemical Engineering Series, McGraw-Hill, New York.

Du, B., Yang, L., Lloyd, C.J., Fang, X., Palsson, B.O., 2019. Genome-scale model of metabolism and gene expression provides a multi-scale description of acid stress responses in Escherichia coli. PLoS Comput. Biol. 15, e1007525. http://dx.doi.org/10.1371/journal.pcbi.1007525.

Edgar, T.F., Himmelblau, D.M., Lasdon, L.S., 2001. Optimization of Chemical Processes, second ed. In: McGraw-Hill Chemical Engineering Series, McGraw-Hill..

Espinel-Ríos, S., Avalos, J.L., 2024. Hybrid physics-informed metabolic cybergenetics: Process rates augmented with machine-learning surrogates informed by flux balance analysis. Ind. Eng. Chem. Res. 63, 6685–6700. http://dx.doi.org/10.1021/acs.iecr.4c00001.

Garcia-Ochoa, F., Gomez, E., 2009. Bioreactor scale-up and oxygen transfer rate in microbial processes: an overview. Biotechnol. Adv 27, 153–176. http://dx.doi.org/10.1016/j.biotechadv.2008.10.006.

Garcia-Ochoa, F., Gomez, E., Santos, V.E., Merchuk, J.C., 2010. Oxygen uptake rate in microbial processes: An overview. Biochem. Eng. J. 49, 289–307. http://dx.doi.org/10.1016/j.bej.2010.01.011.

Garcia-Ochoa, F., Santos, V.E., Gomez, E., 2011. Stirred tank bioreactors. In: Moo-Young, M. (Ed.), Comprehensive Biotechnology. Elsevier, Amsterdam, pp. 179–198. http://dx.doi.org/10.1016/B978-0-08-088504-9.00108-2.

Gombert, A.K., Nielsen, J., 2000. Mathematical modelling of metabolism. Curr. Opin. Biotechnol. 11, 180–186. http://dx.doi.org/10.1016/S0958-1669(00)00079-3.

Gordeeva, Y.L., Glebov, M.B., Gordeev, L.S., 2013. Optimization of microbiological synthesis with nonlinear kinetics of microorganism growth and recycling of substrate and biomass. Theor. Found. Chem. Eng 47, 612–614. http://dx.doi.org/10.1134/S0040579513050175.

Gurobi Optimization, L.L., 2023. Gurobi optimizer reference manual. URL https://www.gurobi.com.

Hansen, S., Gumprecht, A., Micheel, L., Hennemann, H.G., Enzmann, F., Blümke, W., 2022. Implementation of perforated concentric ring walls considerably improves gas-liquid mass transfer of shaken bioreactors. Front. Bioeng. Biotechnol. 10, 894295. http://dx.doi.org/10.3389/fbioe.2022.894295.

Hart, W.E., Watson, J.P., Woodruff, D.L., 2011. Pyomo: modeling and solving mathematical programs in python. Math. Program. Comput. 3, 219–260.

Hebing, L., Tran, F., Brandt, H., Engell, S., 2020. Robust optimizing control of fermentation processes based on a set of structurally different process models. Ind. Eng. Chem. Res. 59, 2566–2580. http://dx.doi.org/10.1021/acs.iecr.9b05504.

Heinzle, E., Biwer, A.P., Cooney, C.L., 2006. Development of bioprocesses. In: Heinzle, E., Biwer, A.P., Cooney, C.L. (Eds.), Development of Sustainable Bioprocesses. Wiley, pp. 11–59. http://dx.doi.org/10.1002/9780470058916.ch2.

Hietala, J., Vuori, A., Johnsson, P., Pollari, I., Reutemann, W., Kieczka, H., 2003. In: Bohnet, M., Ullmann, F. (Eds.), Formic Acid. In: Ullmann's Encyclopedia of Industrial Chemistrye, Wiley-VCH, Weinheim, pp. 1–22. http://dx.doi.org/10.1002/14356007.a12_013.pub3.

Humbird, D., Davis, R., McMillan, J.D., 2017. Aeration costs in stirred-tank and bubble column bioreactors. Biochem. Eng. J. 127, 161–166. http://dx.doi.org/10.1016/j.bej.2017.08.006.

Jabarivelisdeh, B., Carius, L., Findeisen, R., Waldherr, S., 2020. Adaptive predictive control of bioprocesses with constraint-based modeling and estimation. Comput. Chem. Eng. 135, 106744. http://dx.doi.org/10.1016/j.compchemeng.2020.106744.

Jabarivelisdeh, B., Waldherr, S., 2018. Optimization of bioprocess productivity based on metabolic-genetic network models with bilevel dynamic programming. Biotechnol. Bioeng 115, 1829–1841. http://dx.doi.org/10.1002/bit.26599.

Kelly, W.J., 2008. Using computational fluid dynamics to characterize and improve bioreactor performance. Biotechnol. Appl. Biochem. 49, 225–238. http://dx.doi.org/10.1042/BA20070177.

Klamt, S., Gilles, E.D., 2004. Minimal cut sets in biochemical reaction networks. Bioinform. (Oxford, England) 20, 226–234. http://dx.doi.org/10.1093/bioinformatics/btg395.

Knoll, A., Maier, B., Tscherrig, H., Büchs, J., 2005. The oxygen mass transfer, carbon dioxide inhibition, heat removal, and the energy and cost efficiencies of high pressure fermentation. In: Kragl, U. (Ed.), Technology Transfer in Biotechnology. vol. 92, Springer Berlin Heidelberg, Berlin, Heidelberg, pp. 77–99. http://dx.doi.org/10.1007/b98918.

König, A., Neidhardt, L., Viell, J., Mitsos, A., Dahmen, M., 2020. Integrated design of processes and products: Optimal renewable fuels. Comput. Chem. Eng. 134, 106712. http://dx.doi.org/10.1016/j.compchemeng.2019.106712.

Konstantinos, D., Kokossis, A., 2022. Simultaneous synthesis of metabolic and process engineering for the production of muconic acid. ESCAPE32, In: Proceedings 32nd Europ. Symposium Comput. Aided Process Eng., vol. 51, pp. 889–894. http://dx.doi.org/10.1016/B978-0-323-95879-0.50149-1.

Lemmon, E.W., Bell, I.H., Huber, M.L., McLinden, M.O., 2024. Thermophysical properties of fluid systems. In: Linstrom, P., Mallard, W.G. (Eds.), NIST Chemistry WebBook. In: NIST Standard Reference Database, vol. 69, National Institute of Standards and Technology, http://dx.doi.org/10.18434/T4D303.

Liu, S., 2020. Bioprocess Engineering: Kinetics, Sustainability, and Reactor Design, third ed. Elsevier, Amsterdam and Oxford and Cambridge, MA, http://dx.doi.org/10.1016/B978-0-12-821012-3.00018-X.

Luyben, W.L., 2018. Capital cost of compressors for conceptual design. Chem. Eng. Process. 126, 206–209. http://dx.doi.org/10.1016/j.cep.2018.01.020.

Mahadevan, R., Edwards, J.S., Doyle, F.J., 2002. Dynamic flux balance analysis of diauxic growth in Escherichia coli. Biophys. J. 83, 1331–1340. http://dx.doi.org/10.1016/S0006-3495(02)73903-9.

Mandenius, C.F., 2016. In: Mandenius, C.F. (Ed.), Challenges for Bioreactor Design and Operation. In: Bioreactors, Wiley, pp. 1–34. http://dx.doi.org/10.1002/9783527683369.ch1.

Martínez-Salas, E., Martín, J.A., Vicente, M., 1981. Relationship of Escherichia coli density to growth rate and cell age. J. Bacteriol. 147, 97–100. http://dx.doi.org/10.1128/jb.147.1.97-100.1981.

Mayer, F., Haslinger, B., Shpylovyi, A., Weber, A., Windberger, U., Albrecht, B., Hahn, R., Cserjan-Puschmann, M., Striedner, G., 2023. Scale–related process heterogeneities change properties of high–cell–density fermentation broths demonstrated with Escherichia coli b and k–12 strains. J. Chem. Technol. Biotechnol. 98, 1443–1452. http://dx.doi.org/10.1002/jctb.7363.

Mitsos, A., Lemonidis, P., Barton, P.I., 2008. Global solution of bilevel programs with a nonconvex inner program. J. Global Optim. 42, 475–513. http://dx.doi.org/10.1007/s10898-007-9260-z.

Monk, J.M., Lloyd, C.J., Brunk, E., Mih, N., Sastry, A., King, Z., Takeuchi, R., Nomura, W., Zhang, Z., Mori, H., Feist, A.M., Palsson, B.O., 2017. Iml1515, a knowledgebase that computes Escherichia coli traits. Nat. Biotechnol. 35, 904–908. http://dx.doi.org/10.1038/nbt.3956.

Nath, K., Das, D., 2011. Modeling and optimization of fermentative hydrogen production. Bioresour. Technol 102, 8569–8581. http://dx.doi.org/10.1016/j.biortech.2011.03.108.

Negulescu, P.G., Risner, D., Spang, E.S., Sumner, D., Block, D., Nandi, S., McDonald, K.A., 2023. Techno-economic modeling and assessment of cultivated meat: Impact of production bioreactor scale. Biotechnol. Bioeng 120, 1055–1067. http://dx.doi.org/10.1002/bit.28324.

Niebel, B., Leupold, S., Heinemann, M., 2019. An upper limit on Gibbs energy dissipation governs cellular metabolism. Nat. Metab 1, 125–132. http://dx.doi.org/10.1038/s42255-018-0006-7.

Nienow, A.W., 2009. Scale–up, stirred tank reactors. In: Flickinger, M.C. (Ed.), Encyclopedia of Industrial Biotechnology. Wiley, pp. 1–38. http://dx.doi.org/10.1002/9780470054581.eib535.

Nieto, L., Rivera, C., Gelves, G., 2020. Economic assessment of itaconic acid production from Aspergillus Terreus using superpro designer. J. Phys.: Conf. Ser. 1655, 012100. http://dx.doi.org/10.1088/1742-6596/1655/1/012100.

Olsson, L., Rugbjerg, P., Torello Pianale, L., Trivellin, C., 2022. Robustness: linking strain design to viable bioprocesses. Trends Biotechnol 40, 918–931. http://dx.doi.org/10.1016/j.tibtech.2022.01.004.

Orth, J.D., Fleming, R.M.T., Palsson, B.Ø., 2010a. Reconstruction and use of microbial metabolic networks: the core Escherichia coli metabolic model as an educational guide. EcoSal Plus 4, http://dx.doi.org/10.1128/ecosalplus.10.2.1.

Orth, J.D., Thiele, I., Palsson, B.Ø., 2010b. What is flux balance analysis? Nat. Biotechnol. 28, 245–248. http://dx.doi.org/10.1038/nbt.1614.

Parhad, N.M., Rao, N.U., 1974. Effect of pH on survival of Escherichia coli. J. Water Pollut. Control Fed. 46, 980–986, http://www.jstor.org/stable/25038739.

Perry, R.H., Green, D.W., 2008. Perry's Chemical Engineers' Handbook, eighth ed. McGraw-Hill, New York.

Pharkya, P., Maranas, C.D., 2006. An optimization framework for identifying reaction activation/inhibition or elimination candidates for overproduction in microbial systems. Metab. Eng 8, 1–13. http://dx.doi.org/10.1016/j.ymben.2005.08.003.

Pinto, J., Antunes, J., Ramos, J., Costa, R.S., Oliveira, R., 2016. Modeling and optimization of bioreactor processes. In: Pandey, A., Gunasekaran, P., Noronha, S. (Eds.), Current Developments in Biotechnology and Bioengineering. Elsevier, Amsterdam, pp. 89–115. http://dx.doi.org/10.1016/B978-0-323-91167-2.00016-2.

Ploch, T., Zhao, X., Hüser, J., Lieres, E.von., Hannemann-Tamás, R., Naumann, U., Wiechert, W., Mitsos, A., Noack, S., 2019. Multiscale dynamic modeling and simulation of a biorefinery. Biotechnol. Bioeng 116, 2561–2574. http://dx.doi.org/10.1002/bit.27099.

Posten, C., 2018. Integrated Bioprocess Engineering. De Gruyter, http://dx.doi.org/10.1515/9783110315394.

Powell, E.E., Hill, G.A., 2008. Optimization of continuously stirred tank bioreactor design for cost minimization: Effect of microbial species and operating conditions. Int. J. Chem. React. Eng. 6, 00. http://dx.doi.org/10.2202/1542-6580.1642.

Rao, N.N., Lütz, S., Seelbach, K., Liese, A., 2006. Basics of bioreaction engineering. In: Liese, A., Seelbach, K., Wandrey, C. (Eds.), Industrial Biotransformations. Wiley, pp. 115–145. http://dx.doi.org/10.1002/9783527608188.ch5.

Rathore, A.S., Kanwar Shekhawat, L., Loomba, V., 2016. In: Mandenius, C.F. (Ed.), Computational Fluid Dynamics for Bioreactor Design. In: Bioreactors, Wiley, pp. 295–322. http://dx.doi.org/10.1002/9783527683369.ch10.

Richelle, A., David, B., Demaegd, D., Dewerchin, M., Kinet, R., Morreale, A., Portela, R., Zune, Q., von Stosch, M., 2020. Towards a widespread adoption of metabolic modeling tools in biopharmaceutical industry: a process systems biology engineering perspective. NPJ Syst. Biol. Appl. 6, 6. http://dx.doi.org/10.1038/s41540-020-0127-y.

Rosso, L., Lobry, J.R., Bajard, S., Flandrois, J.P., 1995. Convenient model to describe the combined effects of temperature and pH on microbial growth. Appl. Environ. Microbiol. 61, 610–616.

Saur, K.M., Kiefel, R., Niehoff, P.J., Hofstede, J., Ernst, P., Brockkötter, J., Gätgens, J., Viell, J., Noack, S., Wierckx, N., Büchs, J., Jupke, A., 2023. Holistic approach to process design and scale-up for itaconic acid production from crude substrates. Bioeng. (Basel, Switzerland) 10, http://dx.doi.org/10.3390/bioengineering10060723.

Savinell, J.M., Palsson, B.O., 1992. Network analysis of intermediary metabolism using linear optimization. i. development of mathematical formalism.. J. Theor. Biol. 154, 421–454. http://dx.doi.org/10.1016/S0022-5193(05)80161-4.

Schuster, S., Hiletag, C., 1994. On elementary flux modes in biochemical reaction systems at steady state. J. Biol. Syst 02, 165–182. http://dx.doi.org/10.1142/S0218339094000131.

Seidel, S., Maschke, R.W., Werner, S., Jossen, V., Eibl, D., 2021. Oxygen mass transfer in biopharmaceutical processes: Numerical and experimental approaches. Chem. Ing. Tech. 93, 42–61. http://dx.doi.org/10.1002/cite.202000179.

Sieblist, C., Lübbert, A., 2010. Gas holdup in bioreactors. In: Flickinger, M.C. (Ed.), Encyclopedia of Industrial Biotechnology: Bioprocess, Bioseparation, and Cell Technology. Wiley, Hoboken, NJ, pp. 1–8. http://dx.doi.org/10.1002/9780470054581.eib334.

Silverstein, T.P., 2000. Weak vs strong acids and bases: The football analogy. J. Chem. Educ. 77 (849), http://dx.doi.org/10.1021/ed077p849.

Sinner, P., Kager, J., Daume, S., Herwig, C., 2019. Model-based analysis and optimisation of a continuous corynebacterium glutamicum bioprocess utilizing lignocellulosic waste. IFAC-PapersOnLine 52, 181–186. http://dx.doi.org/10.1016/j.ifacol.2019.12.255.

Porto de Souza Vandenberghe, L., Wedderhoff Herrmann, L., de Oliveira Penha, R., Murawski de Mello, A.F., Martínez-Burgos, W.J., Magalhães Junior, A.I., de Souza Kirnev, P.C., de Carvalho, J.C., Soccol, C.R., 2022. Engineering aspects for scale-up of bioreactors. In: Sirohi, R., Pandey, A., Taherzadeh, M.J., Larroche, C. (Eds.), Advances in Bioprocess Engineering. In: Current developments in biotechnology and bioengineering, Elsevier, Amsterdam and Kidlington, Oxford and Cambridge, MA, pp. 59–85. http://dx.doi.org/10.1016/B978-0-323-91167-2.00002-2.

Stephan, P., Kabelac, S., Kind, M., Mewes, D., Schaber, K., Wetzel, T. (Eds.), 2019. VDI-WÄrmeatlas. Springer Berlin Heidelberg, Berlin, Heidelberg, http://dx.doi.org/10.1007/978-3-662-52989-8.

Stephanopoulos, G., Aristidou, A.A., Nielsen, J., 1998. Metabolic Engineering: Principles and Methodologies. Acad. Press, San Diego, Calif.

von Stosch, M., Hamelink, J.M., Oliveira, R., 2016. Hybrid modeling as a qbd/pat tool in process development: an industrial E. coli case study. Bioproc. Biosyst. Eng. 39, 773–784. http://dx.doi.org/10.1007/s00449-016-1557-1.

Straathof, A.J., 2023. Modelling of end-product inhibition in fermentation. Biochem. Eng. J. 191, 108796. http://dx.doi.org/10.1016/j.bej.2022.108796.

Strandberg, L., Köhler, K., Enfors, S.O., 1991. Large-scale fermentation and purification of a recombinant protein from Escherichia coli. Process Biochem. 26, 225–234. http://dx.doi.org/10.1016/0032-9592(91)85004-8.

Tafur Rangel, A.E., Oviedo, A.G., Mojica, F.C., Gómez, J.M., Gónzalez Barrios, A.F. and, 2022. Development of an integrating systems metabolic engineering and bioprocess modeling approach for rational strain improvement. Biochem. Eng. J. 178, 108268. http://dx.doi.org/10.1016/j.bej.2021.108268.

Tepper, N., Shlomi, T., 2010. Predicting metabolic engineering knockout strategies for chemical production: accounting for competing pathways. Bioinform. (Oxford, England) 26, 536–543. http://dx.doi.org/10.1093/bioinformatics/btp704.

Ulonska, K., Skiborowski, M., Mitsos, A., Viell, J., 2016. Early–stage evaluation of biorefinery processing pathways using process network flux analysis. AIChE J. 62, 3096–3108. http://dx.doi.org/10.1002/aic.15305.

Van't Riet, K., 1979. Review of measuring methods and results in nonviscous gas-liquid mass transfer in stirred vessels. Ind. Eng. Chem. Process. Des. Dev. 18, 357–364. http://dx.doi.org/10.1021/i260071a001.

Van't Riet, K., Tramper, J., 1991. Basic Bioreactor Design, vol. 64, Dekker, New York, NY, http://dx.doi.org/10.1002/cite.3306409176.

Vendruscolo, F., Rossi, M.J., Schmidell, W., Ninow, J.L., 2012. Determination of oxygen solubility in liquid media. ISRN Chem. Eng 2012, 1–5. http://dx.doi.org/10.5402/2012/601458.

Villadsen, J., Nielsen, J., Lidén, G., 2011. Bioreaction Engineering Principles, third ed. Springer Science+Business Media LLC, Boston, MA, http://dx.doi.org/10.1007/978-1-4419-9688-6.

Walz, O., Marks, C., Viell, J., Mitsos, A., 2017. Systematic approach for modeling reaction networks involving equilibrium and kinetically-limited reaction steps. Comput. Chem. Eng. 98, 143–153. http://dx.doi.org/10.1016/j.compchemeng.2016.12.014.

Wang, P., Lu, J., Cai, Q., Chen, S., Luo, X., 2021. Analysis and optimization of cooling water system operating cost under changes in ambient temperature and working medium flow. Energies 14 (6903), http://dx.doi.org/10.3390/en14216903.

Wang, J., Wan, W., 2009. Kinetic models for fermentative hydrogen production: A review. Int. J. Hydrog. Energy 34, 3313–3323. http://dx.doi.org/10.1016/j.ijhydene.2009.02.031.

Watson, M.R., 1986. A discrete model of bacterial metabolism. Comput. Appl. Biosci.: CABIOS 2, 23–27. http://dx.doi.org/10.1093/bioinformatics/2.1.23.

Weißgärber, H., 1976. Begasen von Flüssigkeiten in Rührmaschinen (Ph.D. thesis). Bergakademie Freiberg.

Wick, L.M., Quadroni, M., Egli, T., 2001. Short- and long-term changes in proteome composition and kinetic properties in a culture of Escherichia coli during transition from glucose-excess to glucose-limited growth conditions in continuous culture and vice versa. Env. Microbiol 3, 588–599. http://dx.doi.org/10.1046/j.1462-2920.2001.00231.x.

Yawalkar, A.A., Pangarkar, V.G., Beenackers, A.A.C.M., 2002. Gas hold–up in stirred tank reactors. Can. J. Chem. Eng. 80, 158–166. http://dx.doi.org/10.1002/cjce.5450800117.

Zhuang, K., Yang, L., Cluett, W.R., Mahadevan, R., 2013. Dynamic strain scanning optimization: an efficient strain design strategy for balanced yield, titer, and productivity. DySScO strategy for strain design. BMC Biotechnol. 13, 8. http://dx.doi.org/10.1186/1472-6750-13-8.

Ziegler, A.L., Manchanda, A., Stumm, M.D., Blank, L.M., Mitsos, A., 2024. Simultaneous design of fermentation and microbe. AIChE J. http://dx.doi.org/10.1002/aic.18501.

Zwietering, M.H., Wijtzes, T., Rombouts, F.M., Van't Riet, K., 1993. A decision support system for prediction of microbial spoilage in foods. J. Ind. Microbiol. 12, 324–329. http://dx.doi.org/10.1007/BF01584209.